



Available online at www.sciencedirect.com

ScienceDirect

Geochimica et Cosmochimica Acta

Geochimica et Cosmochimica Acta 242 (2018) 143–164

www.elsevier.com/locate/gca

The solubility of monazite (CePO₄), SmPO₄, and GdPO₄ in aqueous solutions from 100 to 250 °C

Alexander P. Gysi a,*, Daniel Harlov b,c, George D. Miron d

Department of Geology and Geological Engineering, Colorado School of Mines, 1516 Illinois Street, Golden, CO 80401, USA
 GeoforschungsZentrum, Telegrafenberg, D-14473 Potsdam, Germany
 Department of Geology, University of Johannesburg P.O. Box 524, Auckland Park 2006, South Africa
 Laboratory for Waste Management, Paul Scherrer Institut, 5232 Villigen PSI, Switzerland

Received 4 April 2018; accepted in revised form 27 August 2018; Available online 12 September 2018

Abstract

Monazite (CePO₄) is a light rare earth element (REE) phosphate occurring as accessory mineral in metamorphic, igneous and sedimentary rocks, and is also a common mineral in REE mineral deposits. Metasomatism of monazite yields important clues about fluid-rock interaction in the crust, in particular, because its compositional variations may enable us to determine conditions of mineralization. The thermodynamic properties of monazite have been determined using several calorimetric methods, but up to the present time only a few solubility studies have been undertaken, which test the reliability of both, the thermodynamic properties of the REE phosphates and associated REE aqueous species. In this study, we have measured the solubility of the monoclinic REE phosphate end-members CePO₄, SmPO₄, and GdPO₄ in aqueous perchloric acid solutions at temperatures from 100 to 250 °C at saturated water vapor pressure (*swvp*). The solubility products (K_{s0}) were determined according to the reaction: REEPO₄ = REE³⁺ + PO₄³⁻.

t(°C)	logK _{s0} (CePO ₄)	$logK_{s0}$ (SmPO ₄)	$logK_{s0}$ (GdPO ₄)
100	-28.4	-28.8	-28.1
150	-29.8	-30.1	-29.4
200	-31.4	-31.7	-31.0
250	-33.4	-33.7	-33.0

Combining available calorimetric data for the REE phosphates with the REE aqueous species from the Supcrt92 (slop98.dat) dataset, yields several orders of magnitude differences when compared with our solubility measurements. We have investigated ways to reconcile these discrepancies and propose a consistent set of provisional thermodynamic properties for REE aqueous species and REE phosphates that reproduce our measured solubility values. To reconcile these discrepancies, we have used the GEMS code package and GEMSFITS for parameter optimization by adjusting the standard Gibbs energy of REEOH²⁺ and REEOH²⁺ at 25 °C and 1 bar. An alternative optimization could involve adjustment of the standard Gibbs energy of REEPO₄(s) and REEOH²⁺. Independently of the optimization method used, this study points to a need to revise the thermodynamic properties of REEOH²⁺ and possibly other REE hydroxyl species in future potentiometric studies. These revisions will have an impact on calculated solubilities of REE phosphates and our understanding of the mobility of REE in natural hydrothermal fluids.

© 2018 Elsevier Ltd. All rights reserved.

Keywords: Monazite; Rare earth elements; Solubility product; Thermodynamics

E-mail address: agysi@mines.edu (A.P. Gysi).

^{*} Corresponding author.

1. INTRODUCTION

Monazite is a common accessory REE phosphate mineral in the Earth's crust, and has proven to be an important geological tracer for geochronology and geothermometry (Gratz and Heinrich, 1997; Heinrich et al., 1997; Pyle et al., 2001; Poitrasson et al., 2002; Spear and Pyle, 2002; Paquette and Tiepolo, 2007). Interest in the properties of REE phosphates has also increased due to the exploration of potential REE mineral resources, where in many cases, the REE phosphate minerals are of hydrothermal origin. These include deposits such as the Browns Range in Australia (Cook et al., 2013; Richter et al., 2018), the Lofdal carbonatite complex in Namibia (Wall et al., 2008), and the giant Bayan Obo deposit in China (Smith et al., 2000). In addition to this economic interest, the stability of REE phosphates and their thermodynamics properties are also of interest for the disposal of radioactive waste in geologic rock formations (Boatner and Sales, 1988).

High temperature and pressure experimental solubility studies have pointed to the possible role of aqueous fluids in controlling the stability of REE phosphates and potential isotope resetting during metasomatism (Ayers and Watson, 1991; Teufel and Heinrich, 1997; Cherniak et al., 2004a, 2004b; Hetherington et al., 2010; Harlov et al., 2011; Williams et al., 2011; Tropper et al., 2011; Grand'homme et al., 2016; Zhou et al., 2016). The importance of metasomatism and compositional changes of monazite has also been recognized in natural systems (Poitrasson et al., 1996; Harlov et al., 2011). Despite these findings, only a few numerical models have been developed for determining the stability of REE phosphates during fluid-rock interaction (Migdisov and Williams-Jones, 2014; Gysi et al., 2015; Migdisov et al., 2016).

Thermodynamic data are available for most REE phosphate endmembers, including enthalpy, entropy, heat capacity and volume data for calculating their properties at high temperatures (Ni et al., 1995; Ushakov et al., 2001; Navrotsky et al., 2015), but only recently have binary solid solutions been measured experimentally. Several studies have shown that these minerals display a non-ideal behavior, despite the REE having similar ionic radii (Popa et al., 2007; Bauer et al., 2016; Geisler et al., 2016; Gysi et al., 2016; Hirsch et al., 2017; Huittinen et al., 2017; Neumeier et al., 2017). These studies have also been complemented by recent ab initio molecular models (Li et al., 2014; Ji et al., 2017). Consideration of solid solutions in the modeling of natural systems will be paramount, as their stability controls the mobility of REE. Before these models can be further developed, a detailed knowledge of the thermodynamic properties of the mineral endmembers and the aqueous REE species is required. Mineral solubility experiments provide a mean to test the validity and compatibility of them both.

The solubility of hydrated REE phosphates (rhabdophane, REEPO₄·0.667H₂O) has been determined at low temperature (Jonasson et al., 1985; Firsching and Brune, 1991; Byrne and Kim, 1993; Liu and Byrne, 1997; Gausse et al., 2016), but only very few studies have been carried out >100 °C (Poitrasson et al., 2004; Cetiner et al., 2005;

Gysi et al., 2015). Experimental difficulties that need to be resolved include the formation of metastable phases at low temperature (Gausse et al., 2016), and the crystallinity and phase stoichiometry of the solids used in the solubility experiments (Cetiner et al., 2005; Gysi et al., 2015). Interpreting these experiments also requires a robust thermodynamic dataset for the aqueous REE species at hydrothermal conditions. Experimental data for aqueous chloride and fluoride complexes permit their stabilities to be determined up to ~ 300 °C (Gammons et al., 1996; Migdisov et al., 2009; Loges et al., 2013; Migdisov et al., 2016). Recent higher temperature experiments permit the constraint of the stability of these species even deeper in the crust (Louvel et al., 2015; Mayanovic et al., 2007, 2009). In contrast, the thermodynamic properties of REE³⁺ ions and hydroxyl complexes are mostly based on theoretical extrapolation using the revised Helgeson-Kirkam-Flowers (HKF) equation-ofstate (Shock and Helgeson, 1988; Wood, 1990; Haas et al., 1995; Shock et al., 1997), which has been implemented in the Supcrt92 database (Johnson et al., 1992). Very few experimental studies are available >100 °C, and to date, only the stability of the Nd hydroxyl complexes was assessed under hydrothermal conditions (Wood et al., 2002; Pourtier and Devidal, 2010). This results in high uncertainties in the predicted thermodynamic properties of the REE aqueous species (Migdisov et al., 2016).

The present work is part of a longer series of experimental studies aimed at constraining the thermodynamic properties of REE phosphates and aqueous REE species in order to build an internally consistent dataset that can be integrated in the MINES thermodynamic database (http://tdb.mines.edu). Here we present new experimental solubility data for the CePO₄, SmPO₄ and GdPO₄ monazite endmembers at 100-250 °C and at saturated water vapor pressure (swvp). Comparison of these experiments with available calorimetric data for the REE phosphates and aqueous REE species from the Supcrt92 database permits revising the standard thermodynamic properties of the aqueous REE species, which seem problematic at hydrothermal conditions. In this study, we also show the application of the GEMSFITS computational optimization tool (Miron et al., 2016, 2017) for adjusting the thermodynamic properties of REE aqueous species during the evaluation of experimental solubility data.

2. SUMMARY OF PREVIOUS WORK AND EXPERIMENTAL CHALLENGES

The REE phosphates occur with a variety of crystal structures, including the tetragonal xenotime (space group *I4/amd*) and the monoclinic monazite (*P2*₁/*n* space group) structures, respectively. The hydrated phase includes rhabdophane (REEPO₄·0.667H₂O), which was previously determined to crystallize in the hexagonal structure (Mooney, 1950) and more recently in the monoclinic (space group C2) structure (Mesbah et al., 2014). Rhabdophane is light REE selective, whereas churchite is another hydrated form that is heavy REE selective (Mooney, 1950; Ni et al., 1995; Mesbah et al., 2014, 2017). As shown in Fig. 1, the solubility of the REE phosphates has been reported in previous

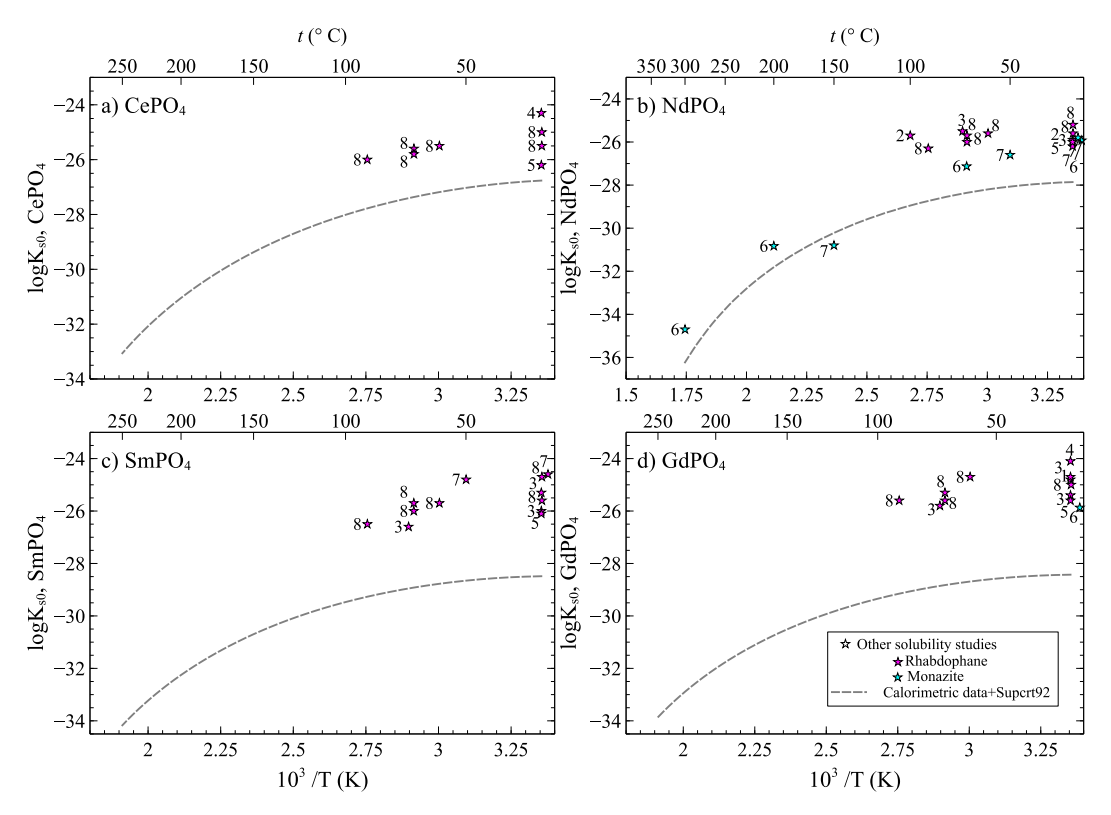


Fig. 1. Comparison of previous measured solubility products ($\log K_{s0}$) of rhabdophane and monazite as a function of temperature. Solubility data are compared to calorimetric data of monazite from Ushakov et al. (2001) combined with aqueous REE³⁺ and PO₄³⁻ species from the Supert92 database (Shock and Helgeson, 1988; Shock et al., 1997). 1: Tananaev and Vasil'eva (1963); 2: Jonasson et al. (1985); 3: Firsching and Brune (1991); 4: Byrne and Kim (1993); 5: Liu and Byrne (1997); 6: Poitrasson et al. (2004); 7: Cetiner et al. (2005); 8: Gausse et al. (2016).

studies conducted at low temperature (<100 °C), but as noted by Cetiner et al. (2005) and Gysi et al. (2015), many of the reported solubility studies did not characterize whether their synthetic solid powders were crystallized in the anhydrous monazite/xenotime structure, or in their hydrated forms.

Hydrothermal NdPO₄ solubility experiments have been carried out by Poitrasson et al. (2004) and Cetiner et al. (2005) at temperatures up to 150 and 300 °C (Fig. 1). The study of Cetiner et al. (2005) reported discrepancies with Poitrasson et al. (2004), which was attributed to possible differences in the crystallinity and hydration of the precipitates used in the experiments. Another problem that was raised by Cetiner et al. (2005), was the possible nonstoichiometric dissolution of REE phosphates, with an excess P attributed to impurities of the synthetic solids used in their experiments. A La, Ce, and Y phosphate synthesis study by Lucas et al. (2004) has confirmed that the precipitation of such powders will lead to an excess of absorbed P that may be removed upon calcination of the solids at 1400 °C. Another approach was taken in the study by Gysi et al. (2015), where mm-sized crystals with the xenotime tetragonal structure were used for hydrothermal solubility experiments performed between 100 and 250 °C. These solids were prepared according to the method of Cherniak et al. (2004a, 2004b), and permit the avoidance of contamination due to P as described above.

Systematic precipitation/dissolution experiments by Gausse et al. (2016) show that rhabdophane will control the solubility at temperatures ≤ 90 °C (Fig. 1). In the study of Gysi et al. (2015), the solubility of the HREE phosphates at >100 °C displayed an overall lower solubility than the hydrated REE phosphates in accordance with the study of Gausse et al. (2016). A similar solubility behavior can be observed for NdPO₄ monazite at >100 °C, whereas at lower temperature its solubility behavior is likely compromised by the stability of rhapdophane (Fig. 1b). Rhabdophane was also controlling the solubility in the La and Nd phosphate precipitation experiments by Roncal-Herrero et al. (2011), and in the precipitation experiments of Du Fou de Kerdaniel et al. (2007) who studied the monazite/rhabdophane transition up to temperatures of 160 °C. The latter study concluded that it is possible to precipitate LaPO₄ with the monazite structure only at temperatures ≥100 °C, whereas CePO₄ would form at ≥120 °C and $PrPO_4$ at ≥ 150 °C (Du Fou de Kerdaniel et al., 2007). Further, Jonasson et al. (1985) pointed out that rhabdophane more easily precipitates/dissolves than monazite at room temperature. Therefore, the observed precipitation behavior of REE phosphates makes it difficult to study the solubility of monazite at <100 °C from oversaturation due to the rhabdophane controlling the solubility of REE at these conditions. This was confirmed in the kinetic study by Arinicheva et al. (2018), who studied the dissolution rates and activation energies of rhabdophane-(La) and monazite-(La), and reported the formation and dissolution of a thin layer of rhadophane-(La) forming at the monazite surface at <90 °C. This lower stability of monazite <100 °C, could explain the observed discrepancies in previous experiments carried out at these conditions (Fig. 1). It is currently, however, unclear under which exact conditions the different monazite endmembers are replaced by metastable phases in hydrothermal aqueous solutions <100 °C.

The hydrothermal solubility experiments of Gysi et al. (2015) could avoid these problems by approaching equilibrium from undersaturation at temperatures between 100 and 250 °C. This method was applied successfully in reproducing the expected Gibbs energies for DyPO₄ and YbPO₄, whereas several orders-of-magnitude discrepancies were observed between the experimentally derived solubility constants for ErPO₄ and YPO₄ in comparison to the calculated values from the literature data. The latter are obtained using available calorimetric data for the minerals combined with aqueous species data from the Supert92 database (Shock and Helgeson, 1988; Haas et al., 1995). Further, comparison of previous low temperature solubility data for CePO₄, SmPO₄, and GdPO₄ (Jonasson et al., 1985; Firsching and Brune, 1991; Byrne and Kim, 1993; Liu and Byrne, 1997) with the available literature data indicates a large difference in retrieved solubility products (Fig. 1). These discrepancies need to be addressed, and point to a need to revise the thermodynamic properties of either the REE phosphate endmembers and/or the properties of aqueous REE3+ and hydroxyl complexes from the Supcrt92 database.

3. MATERIALS AND METHODS

3.1. Starting materials

Individual crystals of monoclinic monazite of CePO₄, SmPO₄, and GdPO₄ were grown from a melt flux utilizing the synthesis techniques outlined in Cherniak et al. (2004a, 2004b). For the synthesis of the crystals, a finegrained powder of hydrated REE phosphates was first precipitated by mixing a solution containing dissolved REE (NO₃)₃ with a NH₄H₂PO₄ solution. These precipitates were then dried, powdered, and consequently mixed with a Pb-free flux of Na₂CO₃ and MoO₃ (molar ratio of 75Na₂CO₃:25MoO₃:REEPO₄). This mix was then placed in a Pt crucible with a loose cover and heated up to 1375 °C in air, and left (soaked) for 15 hours. The flux was then slowly cooled at a rate of 3 °C/hour to 870 °C over approximately 5 days. The flux and embedded REE phosphate crystals were then boiled in successive beakers of distilled H₂O until the crystals were freed from the flux. The inclusion-free, mm-sized, REE endmember crystals, typically used in the solubility experiments are shown in Fig. 2 together with representative EDS spectra.

The experimental starting solutions were prepared using trace metal grade (Fisher Scientific) perchloric (HClO₄) and phosphoric (H₃PO₄) acid. The acidic (pH \sim 2) perchloric

aqueous solutions used in our study allowed us to increase the solubility of the LREE phosphates and avoid complexation of the REE with additional ligands, thereby ensuring that the latter occurred dominantly as free REE³⁺ and REE(OH)²⁺ species depending on temperature. Perchloric acid was first added at room temperature to 400 ml Milli-Q water (18 M Ω -cm) to reach a pH of 2, to control the initial ClO₄⁻ concentration. The initial P concentration was constrained by adding an aliquot of 100 μ l of a H₃PO₄ stock solution to the 400 ml HClO₄ solution. Sample holders used in the experiments were made of Ti foil (99.7% purity; Alfa Aesar).

3.2. Experiments

Solubility experiments were carried out in 45 ml batchtype reactors (Parr 4744, Teflon-lined stainless steel) at 100, 150, 200 and 250 °C at swvp for up to 21 days. Each reactor was first loaded with a hand-made titanium sample holder containing a synthetic mm-sized REE phosphate crystal and 25 ml of the starting aqueous HClO₄-H₃PO₄ solution. The autoclaves were purged of air with a stream of dry nitrogen and then sealed, and rapidly heated in a Cole-Parmer muffle furnace (EW-33858-70). The temperature was recorded with an Omega® temperature logger using a K-type thermocouple located at the center of the furnace and the experimental temperature was maintained within 0.5 °C. After the experiments, the autoclaves were quenched in cold water for <20 min (Gysi et al., 2015). The experimental solution was then pipetted out and diluted (1/6 per volume) in a 2% HNO₃ (trace metal grade, Fisher Scientific) blank matrix solution for the analysis of P and REE concentrations using solution inductively coupled plasma mass spectrometry (ICP-MS). After the experiments, the sample holders were extracted and the walls of the reactors washed with a concentrated sulfuric acid solution (trace metal grade, Fisher Scientific), and soaked overnight with milli-Q water before starting any new experiments. The experimental uncertainty was assessed by carrying out a series of duplicate experiments for a selected set of solubility experiments at different temperatures.

The experimental design is similar to the one used by Gysi et al. (2015) for the solubility of xenotime, approaching equilibrium from undersaturation. Addition of P to the initial aqueous solutions permits the constraint of the concentrations of dissolved REE phosphate to values in the lower ppb range. This methods permits the avoidance of the precipitation of any additional metastable phase that could control solubility (Gausse et al., 2016), since all the experiments are carried out >100 °C. The major advantage of using mm-sized crystals over fine powders is the slightly slower dissolution rates of these solids (i.e., few days equilibration time), which avoids reaction of the crystals with the aqueous solution upon rapid (<20 min) quenching. In addition, the retrograde solubility of the REE phosphates will ensure that precipitation of solids will be avoided upon quenching.

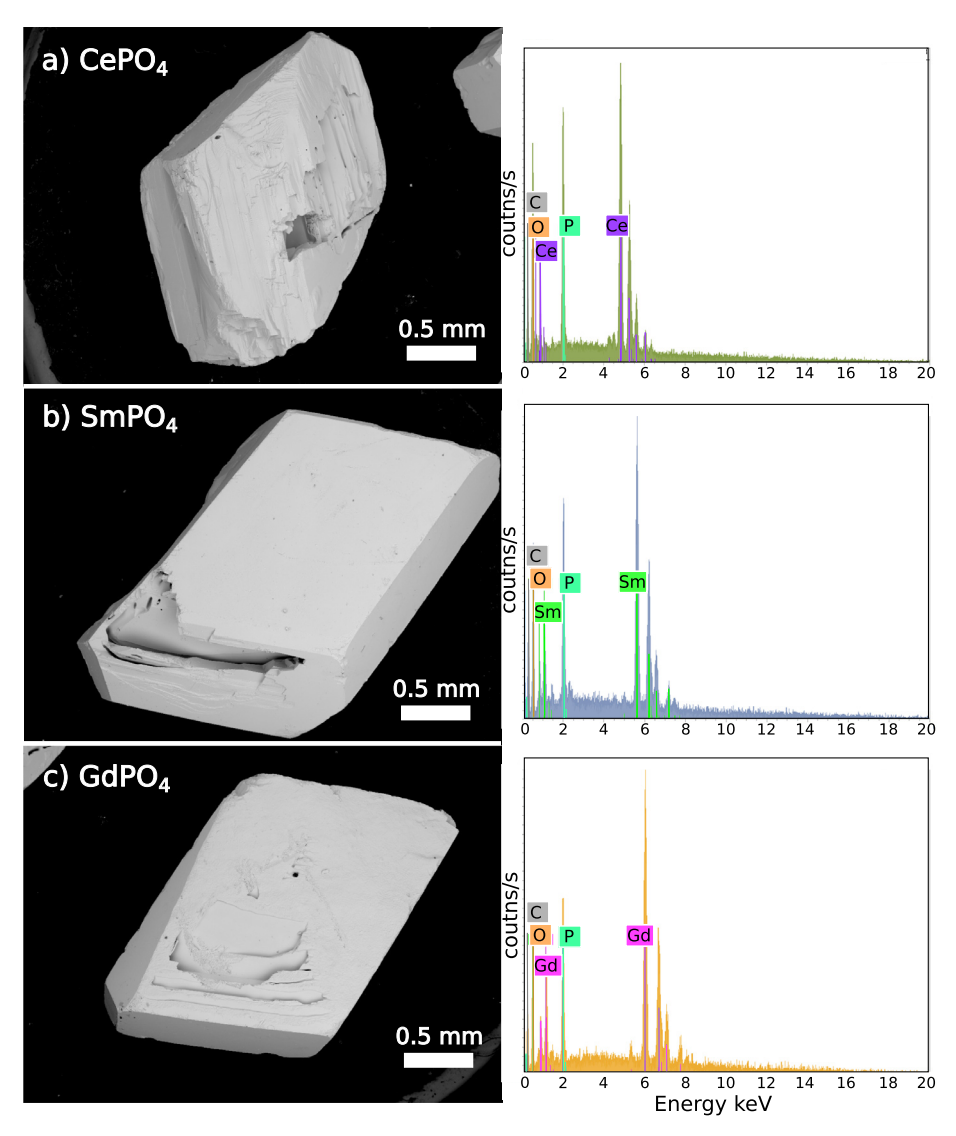


Fig. 2. Field emission scanning electron photomicrographs and EDS spectra for synthesized pure monazite crystals of (a) CePO₄, (b) SmPO₄ and (c) GdPO₄. The synthesized solids display well developed crystal faces with a typical monoclinic structure ($a \neq b \neq c$, $\alpha = \gamma = 90^{\circ}$, $\beta \neq 90^{\circ}$).

3.3. Analytical

The synthetic REE phosphate crystals used in the experiments were studied using a TESCAN MIRA3 LMH Schottky field emission scanning electron microscope (FESEM) equipped with a Bruker energy dispersive spectrometer (EDS). Carbon-coated samples were analyzed using an acceleration voltage of 25 kV and a working distance of 9.5 mm for backscattered imaging.

The pH of the starting experimental solutions was measured at room temperature using a combination electrode (60260010 unitrode, Metrohm) and a Metrohm 913 pH meter. The electrode was calibrated using commercial buffer solutions (Fisher Scientific; pH 2, 4 and 7 buffer solutions), which enabled measurements to be made to a precision of 0.02 pH units.

The quenched experimental solutions (Table A1) were analyzed using a Perkin Elmer NexION 300Q quadrupole ICP-MS. Standards and samples were all diluted using 2% HNO₃ (Fisher Scientific, trace metal grade) blank solutions and spiked with In (SCP Science, NIST traceable certified standards) as an internal standard for drift correction. The calibration was carried out using a multi-element REE standard, a P standard and single REE (La and Ce) standards (SCP Science, NIST traceable certified standards). The latter were used for interference corrections due to oxide (18O and 16O) formation. Analyzed samples were blank-subtracted after drift correction. Phosphorus is difficult to analyze in the lower ppb range due to an interference with nitrogen (14N16OH and 15N16O) from the 2% HNO₃ blank matrix resulting in high background counts. To avoid this problem, standard curves were constructed with concentrations of above 10 ppb, and the P concentration ranges of the diluted experimental solutions corresponded to values of $\sim 100-400$ ppb. In this concentration range, the linear regression coefficients (R²) for P were 0.999. The analytical precision of triplicate ICP-MS runs based on a 95% confidence level was 3% for P and <1% for Ce, Sm and Gd. The limit of detection (LOD) was determined from the 3σ (standard deviation) value of the blank, which was established by multiple measurements of the total procedural blank. The LOD values were 4 ppb for P, 89 ppt for Ce, 10 ppt for Sm, and 23 ppt for Gd.

4. DATA TREATMENT

4.1. Speciation calculations

Aqueous speciation calculations were carried out using the GEMS code package v.3 (Wagner et al., 2012; Kulik et al., 2013). Thermodynamic properties for the aqueous species were calculated at the temperature of interest using the revised HKF equation-of-state (Helgeson et al., 1981; Shock and Helgeson, 1988; Tanger and Helgeson, 1988; Shock et al., 1992). The properties of H₂O were calculated from the IAPS-84 equation-of-state (Kestin et al., 1984). Thermodynamic data for the aqueous species considered in the speciation calculations are listed in Table 1, and were taken from Shock and Helgeson (1988), Shock et al. (1989), Haas et al. (1995), and Shock et al. (1997), hereafter referred to Supcrt92.

The activities of the aqueous ions of interest (REE³⁺, REEOH²⁺, H⁺, H₃PO₄⁰, H₂PO₄⁻, HPO₄²⁻, and PO₄³⁻; other species considered are listed in Table 1) were determined at the experimental temperature and *swvp* using the concentra-

Table 1 Aqueous species considered in the initial calculations and sources of thermodynamic data from Supert92 (Johnson et al., 1992), slop98.dat.

Species	References
Ce-species Ce ³⁺ Ce(OH) ₃ , Ce(OH) ₂ +, CeOH ²⁺ , Ce(OH) ₄ -	1, 2
Sm -species Sm^{3+} $Sm(OH)_3^0$, $Sm(OH)_2^+$, $SmOH^{2+}$, $Sm(OH)_4^-$	1, 2 3
Gd -species Gd^{3+} $Gd(OH)_3^0$, $Gd(OH)_2^+$, $GdOH^{2+}$, $Gd(OH)_4^-$	1, 2 3
$Major$ P-species $H_3PO_4^0$ $H_2PO_4^-$, HPO_4^{2-} , PO_4^{3-}	4 1, 2
Minor P-species $\begin{array}{l} \text{Minor P-species} \\ H_2P_2O_7^{2-}, \ H_3P_2O_7^{-}, \ H_4P_2O_7^{0}, \ HP_2O_7^{3-}, \ P_2O_7^{4-} \end{array}$	1, 2
Other species OH ⁻ , H ⁺ ClO ₄ ⁻	1, 2 1, 2

Supcrt92, slop98.dat: ¹Shock et al. (1997), ²Shock and Helgeson (1988), ³Haas et al. (1995), ⁴Shock et al. (1989).

tions of REE and P from the quenched experimental solutions, and the ClO_4^- concentrations calculated from the measured pH values of 2.00 from the experimental starting solutions (Appendix A). The activity coefficients (γ_i) of the neutral species were set to unity, and the γ_i of water was calculated using the osmotic coefficient (Helgeson et al., 1981). The γ_i of the charged aqueous species were calculated using the extended Debye-Hückel equation (Robinson and Stokes, 1968),

$$log\gamma_{i} = -\frac{Az_{i}^{2}\sqrt{I}}{1+\mathring{a}B\sqrt{I}} + \Gamma_{\gamma} + b_{\gamma}I \tag{1}$$

where the effective ionic strength I, is given by,

$$I = 1/2 \sum_{i} m_i z_i^2 \tag{2}$$

A and B are the Debye-Hückel parameters (Helgeson and Kirkham, 1974; Helgeson et al., 1981), Γ_{γ} is a mole fraction to molality conversion factor, b_{γ} is the extended term parameter, a_i is the ion size parameter, m_i is the molal concentration and z_i is the charge of the *i*th aqueous species. The value b_{γ} is an empirical parameter that depends on the background electrolyte, and was determined up to 250 °C in the experimental study by Migdisov and Williams-Jones (2007). For HClO₄/NaClO₄ aqueous solutions, the b_{γ} parameter was determined to have a value of 0.21. The ion size parameters of individual ions were taken from Migdisov and Williams-Jones (2007) for ClO₄ (4.5 Å) and from Kielland (1937) for other ions.

4.2. Solubility constant (K_s) calculations

The solubility constants (K_s) of the REE phosphates are described by the following dissolution reactions:

REEPO₄(s) = REE³⁺ + PO₄³⁻ (
$$K_{S0}$$
) (3)

$$REEPO_4(s) + H^+ = REE^{3+} + HPO_4^{2-}$$
 (K_{S1}) (4)

REEPO₄(s) + 2H⁺ = REE³⁺ + H₂PO₄⁻ (
$$K_{S2}$$
) (5)

$$REEPO_4(s) + 3H^+ = REE^{3+} + H_3PO_4^{\ 0} \quad (K_{53})$$
 (6)

At a pH value of ~ 2.0 , which corresponds to the experimental conditions (Table A1), the major phosphate species were H₃PO₄⁰ and H₂PO₄⁻, with H₃PO₄⁰ as the dominant species. We therefore first determined K_{s3} at the experimental temperature using Reaction (6), with the equilibrium constant given by,

$$\mathbf{K}_{s3} = \frac{a_{H_3PO_4^0} \times a_{REE^{3+}}}{a_{H^+}^3} \tag{7}$$

where a is the activity of REE³⁺, H₃PO₄⁰ and H⁺, respectively. The ionization reactions of orthophosphoric acid as a function of proton (H⁺) activity can be described by,

$$H_3PO_4^{\ 0} = H^+ + H_2PO_4^{\ -} \quad (K_1)$$
 (8)

$$H_2PO_4^- = H^+ + HPO_4^{2-}$$
 (K₂) (9)

$$HPO_4^{2-} = H^+ + PO_4^{3-} \quad (K_3)$$
 (10)

where K_1 , K_2 and K_3 are the first, second and third ionization constants for orthophosphoric acid (Table A2). The solubility product for Reaction (3) can be calculated by

combining Eq. (7) with the ionization constants of orthophosphoric acid according to,

$$\mathbf{K}_{s0} = \mathbf{K}_{s3} \times \mathbf{K}_1 \times \mathbf{K}_2 \times \mathbf{K}_3 \tag{11}$$

where K_{s0} represents the solubility product with the activity relationship,

$$K_{s0} = a_{REE^{3+}} \times a_{PO^{3-}} \tag{12}$$

4.3. Parameter optimization calculations

To regress the standard molal Gibbs energies of aqueous REE species, we used the GEMSFITS code (Miron et al., 2015), which uses the GEMS code package (Kulik et al., 2013) for chemical equilibria and speciation calculations and the TSolMod library of activity models and equations of state parameters (Wagner et al., 2012). The starting values for the standard thermodynamic properties of REE aqueous species were from Shock and Helgeson (1988), Haas et al. (1995), and Shock et al. (1997). The HKF parameters, entropies, heat capacities, and molar volumes listed in Table A3 were kept constant during the optimization. Only the standard molal Gibbs energy at 25 °C and 1 bar was optimized for either REE3+ and REEOH2+ (mode I), or REEOH²⁺ and the REE phosphate minerals (mode II). The standard thermodynamic properties for REE phosphates were taken from the calorimetric measurements of Ushakov et al. (2001), Thiriet et al. (2004, 2005), and Popa and Konings (2006) as listed in Table 2. Evaluation of the experimental solubility data (Table A1) for the optimization was conducted using the activity models, speciation and thermodynamic data described above.

5. EXPERIMENTAL RESULTS

5.1. Kinetic experiments

Before retrieving the solubility products of the REE phosphates, kinetic experiments were carried out to test whether equilibrium was attained in the experiments. For this purpose, the solubility of CePO₄ was measured in a series of experiments at 100 °C and *swvp* for a duration of 1 to 21 days. These experiments were conducted at the lowest

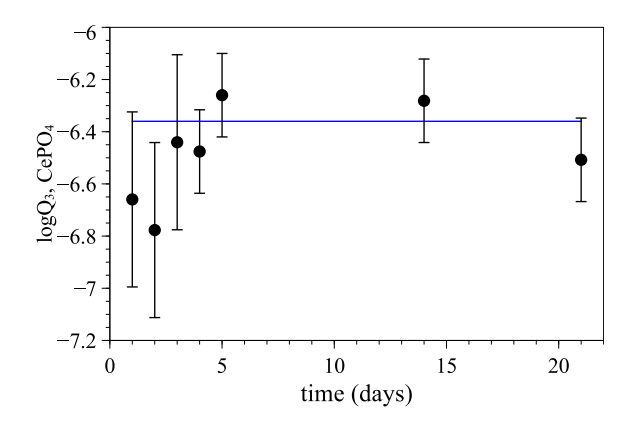


Fig. 3. Results from kinetic experiments at $100\,^{\circ}\text{C}$ and swvp showing the time required for Ce to reach steady state concentrations after ~ 5 days. This is displayed as the logarithm of the reaction quotient (Reaction (6) and Eq. (7)) as a function of time (days).

experimental temperature for ascertaining that dissolution kinetics will not affect the retrieved solubilities.

The results of the kinetic experiments are shown in Fig. 3 as reaction quotients (Q_{s3}) calculated using Reaction (6) and retrieved activities of the aqueous species (Table A1). The reaction quotients for CePO₄ indicate that the experimental solutions had very low Ce concentrations after 1-2 days, followed by a rapid increase after 3 days to approach equilibrium with the CePO₄ crystals. After 5, 14 and 21 days, Q_{s3} varied only within the experimental uncertainty, which indicates that after ~5 days the measured Ce concentrations reached steady state values. This is in line with similar solubility experiments carried out with YPO₄ crystals, where the experiments reached equilibrium at 100 °C after \sim 10 days reaction time (Gysi et al., 2015). This method has also proven to be valid for other similar solubility studies, which suggest approach to equilibrium after only few days at the experimental conditions (Migdisov et al., 2009; Migdisov et al., 2011; Loges et al., 2013). Additional evidence that equilibrium was reached in these experiments is provided by the good agreement in the experimental uncertainty obtained from selected duplicate experiments repeated for the same isotherms (Table 3).

Table 2 Standard thermodynamic properties of REE phosphates at reference conditions (T_r, P_r) of 298.15 K and 1 bar from calorimetric studies. The heat capacity function is described by $Cp^\circ = a + bT + c/T^2$, with T in Kelvin.

	$\Delta_f G^0_{\mathrm{Tr,Pr}}$ kJ/mol	Δ _/ H ⁰ _{Tr,Pr} kJ/mol	S [°] _{298.15 K} J/mol/K	$V_{\rm m}$ cm ³ /mol	$\mathop{\mathrm{Cp}^{\circ}}_{\mathrm{J}\;\mathrm{mol}^{-1}\mathrm{K}^{-1}}$	a	b	С
CePO ₄	-1847.53	-1967.8 ^a	119.97 ^b	4.516°	106.43 ^d	125.209	0.0278936	-2.40858e+06
$SmPO_4$	-1846.90	-1965.7^{a}	122.49 ^b	4.281°	105.60 ^e	133.125	0.0234677	-3.06879e+06
$GdPO_4$	-1844.47	-1962.0^{a}	124.60 ^b	4.201°	102.21 ^d	133.237	0.0127933	-3.09720e+06

^a Ushakov et al. (2001), oxide melt calorimetry using crystals grown from melt flux.

^b Thiriet et al. (2004, 2005), hybrid adiabatic relaxation calorimetry and differential scanning calorimetry (DSC). CePO₄, and GdPO₄ experiments were combined with crystal-field energy calculations for determining entropy of SmPO₄.

^c Ni et al. (1995).

^d Popa et al. (2006), drop calorimetry Cp function for LaPO₄, CePO₄ and GdPO₄.

^e Popa and Konings (2006), drop calorimetry Cp function for SmPO₄ and EuPO₄.

Table 3 Values of the logarithm of the solubility product (log K_{s0}) of REE phosphates determined experimentally at temperature (t) and swvp.

t (°C)	$\log K_{s0}$ (CePO ₄)	$1\sigma^{a}$	$\log K_{s0} (\mathrm{SmPO_4})$	lσ ^a	$\log K_{s0} (\mathrm{GdPO_4})$	$1\sigma^a$
100	-28.44	±0.16	-28.29	±0.11 ^b	-27.98	±0.05
150	-29.48	± 0.01	-29.22	± 0.27	-28.88	± 0.12
200	-30.61	$\pm 0.11^{b}$	-29.85	$\pm 0.11^{b}$	-30.28	± 0.14
250	-32.22	± 0.14	-31.14	$\pm 0.11^{b}$	-31.25	± 0.01

Aqueous speciation calculations were carried out using the aqueous species listed in Table 1 and K_{s0} was calculated using Eqs. (7) and (11) using the data in Tables A1 and A2.

5.2. Solubility products (K_{s0})

The solubility products of the REE phosphates were retrieved from the measured concentrations of REE and P in the quenched experimental solutions (Table A1) and calculated activities according to Eqs. (7) and (11). The resulting values of the logarithm of K_{s0} for CePO₄, SmPO₄ and GdPO₄ are listed in Table 3 and shown in Fig. 4. The solubility of the REE phosphates is retrograde between 100 and 250 °C, with log K_{s0} values varying 2–4 orders of magnitude. Duplicate experiments display excellent reproducibility for CePO₄ and GdPO₄ with experimental uncertainties in $\log K_{s0}$ generally <0.2. One duplicate experiment for the solubility of SmPO₄ indicates a higher uncertainty of 0.3. However, the calculated upper bound of uncertainties is 0.11 at the 95% confidence level based on 9 duplicate experiments at temperatures between 100 and 250 °C. An experimental uncertainty of <0.2 in retrieved $\log K_{s0}$ values is similar to the uncertainty observed for similar REE phosphate solubility experiments carried out by Gysi et al. (2015).

Values of $\log K_{s0}$ do not vary linearly with 1/T, indicating that the enthalpy of reaction varies with temperature. The experimental data were fit to an equation of the form,

$$logK = A + B \times T + \frac{C}{T} + Dlog(T) \tag{13} \label{eq:13}$$

in which T is the temperature in Kelvin and the significance of the coefficients A, B, C, D are given further below. For four isotherms between 100 and 250 °C, only the first three coefficients were needed for the initial fit of our experimental data, yielding regression coefficients (R²) between 0.970 and 0.996 (fit1, Table 4). Extrapolation of the fits to 25 °C leads to large uncertainties at the 95% confidence level (Fig. 4).

5.3. Comparison to previous studies

To better constrain the extrapolations of $\log K_{s0}$ to 25 °C, our data were compared to results from other available solubility studies. Previous investigations of the thermodynamic properties of CePO₄, SmPO₄ and GdPO₄ have been carried out at low temperature conditions where the solubility experiments are controlled by the stability of rhabdophane (Tananaev and Vasil'eva, 1963; Firsching and Brune, 1991; Byrne and Kim, 1993; Liu and Byrne, 1997;

Cetiner et al., 2005; Gausse et al., 2016). Calorimetric methods were used to determine heat capacity, entropy and enthalpy of REE phosphates (Ushakov et al., 2001; Thiriet et al., 2004; Thiriet et al., 2005; Popa and Konings, 2006; Popa et al., 2006). These experimental data are compared to our experimental fits in Fig. 4. To calculate solubilities, the calorimetric data for REE phosphates listed in Table 2 were combined with standard thermodynamic properties of REE³⁺ and PO₃⁴⁻ species of Supcrt92 (Shock and Helgeson, 1988; Shock et al., 1997).

Our values of $\log K_{s0}$ for CePO₄ extrapolated to 25 °C (Fig. 4a) are similar to, but slightly lower than, the values calculated from the calorimetric data combined with Supert92. For the estimated uncertainty at the 95% confidence level, our value at 25 °C is indistinguishable from the calculated calorimetric data. In contrast, the rhadophane solubility constants reported by Byrne and Kim (1993) and Liu and Byrne (1997) are systematically higher by several orders of magnitude. Comparison of our data with the rhabdophane solubility experiments of Gausse et al. (2016), indicates that rhabdophane (CePO₄·0.667H₂O) has systematically a higher solubility than monazite (CePO₄), but displays a similar trend of decreasing solubility with increasing temperature. In the study of Byrne and Kim (1993), fine REE phosphate powders were synthesized at room temperatures, and values were reported as LnPO₄·nH₂O, indicating that these authors synthesized rhapdophane, which was also used in the study of Liu and Byrne (1997). To our knowledge, our study is therefore the first to report data on the solubility of CePO₄ with the monazite structure between 100 and 250 °C and at swvp.

The solubility product of SmPO₄ extrapolated to 25 °C (Fig. 4b), is higher in our study than the values calculated from calorimetric data, and again lower than solubility studies of rhabdophane (SmPO₄·0.667H₂O) reported by Gausse et al. (2016). For the estimated uncertainty at the 95% confidence level, our value at 25 °C is indistinguishable from the re-calculated calorimetric data. The solubility of the phases synthesized by Firsching and Brune (1991) are similar to the study by Gausse et al. (2016), but the solids synthesized in the former study have not been well documented. The study by Liu and Byrne (1997) confirmed, however, that this synthesis method produced hydrated REE phosphates with the rhabdophane structure, which explains their higher measured solubilities. The study of

^a The uncertainty (σ) is the standard deviation of the mean based on duplicate experiments.

^b Calculated experimental uncertainty on the 95% confidence level (upper bound), based on 1σ obtained from available duplicate experiments.

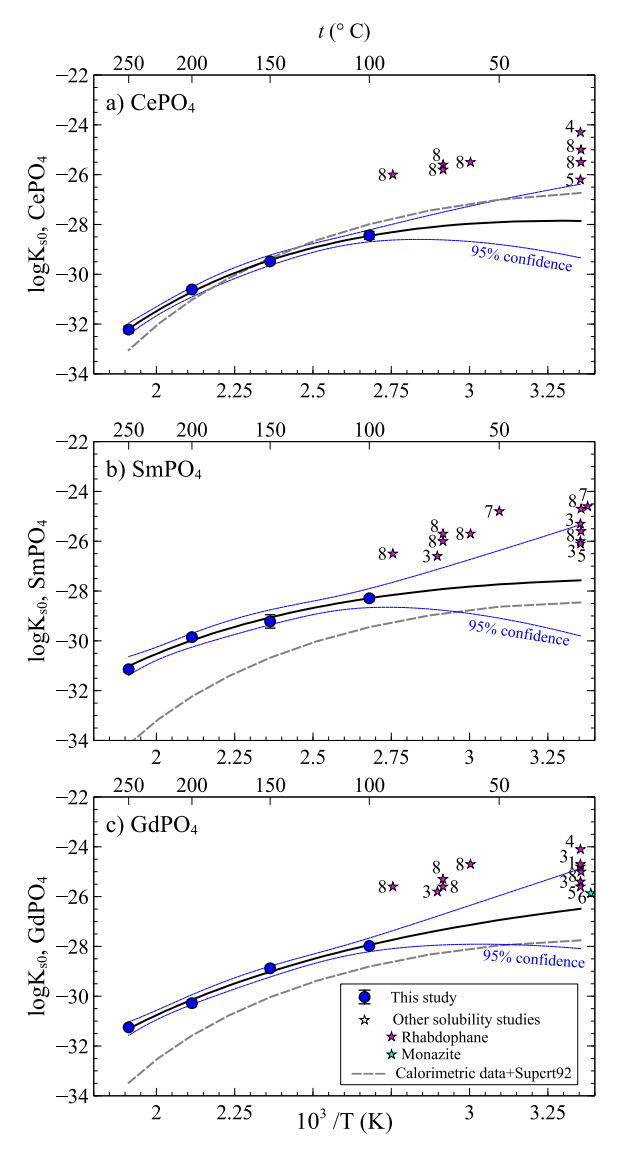


Fig. 4. Plots showing the logarithm of the solubility products of REE phosphates (log K_{s0}) vs. 1/T calculated from the experimental data collected in this study for temperatures between 100 and 250 $^{\circ}$ C together with non-linear fits (Eq. (13)) extrapolated to 25 °C at the 95% confidence interval (blue lines). The experimental data and coefficients from the regressions (fit 1) are reported in Tables 3 and 4. Solubility data are compared to calorimetric data of monazite from Ushakov et al. (2001) combined with aqueous REE³⁺ and PO₄³⁻ species from the Supert92 database (Shock and Helgeson, 1988; Shock et al., 1997). Also shown are experimentally determined values of log K_{s0} (numbered symbols) from other solubility studies. 1: Tananaev and Vasil'eva (1963); 2: Jonasson et al. (1985); 3: Firsching and Brune (1991); 4: Byrne and Kim (1993); 5: Liu and Byrne (1997); 6: Poitrasson et al. (2004); 7: Cetiner et al. (2005); 8: Gausse et al. (2016). The error bars or symbol sizes represent the 1σ values from duplicate experiments. (For interpretation of the references to color in this figure legend, the reader is referred to the web version of this article.)

Cetiner et al. (2005) also determined the solubility of rhabdophane-(Sm) powders, with higher solubilities than in our study.

The solubility product for GdPO₄ (Fig. 4c) displays a similar trend as SmPO₄, where the extrapolated log *K*₅₀ to 25 °C are higher than the values calculated from calorimetric data. The better uncertainty of the extrapolated fit calculated on the 95% confidence level indicates that the values calculated from calorimetric data plots and the measured solubility data for rhapdophane (GdPO₄·0.667H₂O) mostly plot within this confidence field at 25 °C. The solubilities of rhabdophane synthesized by Firsching and Brune (1991) are similar to the ones measured by Gausse et al. (2016), whereas the solubility data of Tananaev and Vasil'eva (1963), Byrne and Kim (1993), and Liu and Byrne (1997) display larger deviations.

6. RESOLVING DISCREPANCIES BETWEEN THERMODYNAMIC PROPERTIES OF MINERALS, AQUEOUS SPECIES AND SOLUBILITY EXPERIMENTS

6.1. Constraining experimental fits to 298.15 K and 1 bar

Since extrapolated $\log K_{s0}$ at 25 °C display relatively large uncertainties at the 95% confidence interval (Fig. 4), the fits need to be better constrained, which can be done using available calorimetric data for the minerals. In a first step, the standard enthalpy of Reaction (3), hence the enthalpy of formation $(\Delta_f H_{Tr,Pr}^0)$ of the REE phosphates, can be calculated using the fitted coefficients of the log K_{s0} function (see Fit 1 in Table 4) and the Van't Hoff relation (Appendix B). The $\Delta_t H_{Tr,Pr}^0$ values obtained by the fit of the solubility experiments are more positive by 7 to 27 kJ/mol for SmPO₄ and GdPO₄, and more negative by 14 kJ/mol for CePO₄ in comparison to the calorimetric values of Ushakov et al. (2001). In the second step, we used the values of Ushakov et al. (2001) for the enthalpy at 298.15 K to constrain the parameter C in Eq. (13). This allowed us to refit the experimental data using four coefficients (Fit 2 in Table 4). In the third step, we used the calorimetric data of Thiriet et al. (2004, 2005) for entropy at 298.15 K to constrain parameter A (Fit 3 in Table 4). The constrained fits (Fit 2 optimized for enthalpy; Fit 3 optimized for entropy) are compared in Fig. 5. This constrained fitting for GdPO₄ made the slopes of the $\log K_{\rm s0}$ vs. 1/T curves more consistent with those based on the calorimetric data at temperatures between 25 and 100 °C, whereas for CePO₄ and SmPO₄, the resulting slopes still display deviations.

Combining the values of the corrected mineral $\Delta_J H_{Tr,Pr}^0$ based on these fits and their standard properties (Table 2, Cp function) with the aqueous REE³⁺ and PO₄³⁻ properties from Supert92, did not permit to reconcile the solubility measurements with the calorimetric data (Fig. 5; Optimized at 298.15 K, 1 bar). This is in contrast to the previous study of Gysi et al. (2015), were correcting the $\Delta_J H_{Tr,Pr}^0$ values of the minerals permitted to reconcile these data. Discrepancies become large at temperatures >100 °C, with 1–3 orders of magnitude differences in comparison to our measured experimental values. We have investigated ways to reconcile these discrepancies and propose a consistent set of thermodynamic properties for aqueous species and minerals, that

Table 4 Coefficients for the temperature (T in K) dependence of the solubility products ($\log K_{s0}$) of REE phosphates determined from regression of the experimental values listed in Table 3.

		$\log K = A + B'$	T + C/T + Dlog(T))	\mathbb{R}^2	$\log K_{\rm s0}$	$^{\mathrm{c}}\Delta_{f}\mathrm{H}^{0}{}_{Tr,Pr}$	${}^{\mathbf{d}}\mathbf{S}^{0}{}_{Tr}$
	A	В	С	D		(298.15 K)	(kJ/mol)	(J/mol/K)
Fit 1								
$\log K_{\rm s0}$ (CePO ₄)	0.968	-0.0474	-4.384E+03	_	0.996	-27.86	-1981.5	95.5
$\log K_{s0} (SmPO_4)$	-12.45	-0.0283	-1.987E + 03	_	0.970	-27.56	-1958.8	127.8
$\log K_{s0} (\mathrm{GdPO_4})$	-15.97	-0.0265	-784.5E+02	_	0.991	-26.48	-1934.8	180.0
Fit 2 optimized for I	ΔH							
$\log K_{\rm s0}$ (CePO ₄)	-229.46	-0.0912	3.757E+03	87.48	0.996	-27.61	-1967.8^{a}	136.6
$\log K_{s0} (SmPO_4)$	3.94	-0.0286	$-3.047E \pm 03$	-5.24	0.969	-27.77	-1965.7^{a}	108.7
$\log K_{s0} (\mathrm{GdPO_4})$	439.74	0.0602	-1.691E + 04	-172.96	0.993	-26.99	-1962.2^{a}	97.8
Fit 3 optimized for I	ΔS							
$\log K_{\rm s0}$ (CePO ₄)	-145.57	-0.0756	7.435E+02	55.73	0.996	-27.72	-1973.4	120.0 ^b
$\log K_{s0} (SmPO_4)$	-57.69	-0.0397	-7.876E + 02	17.99	0.969	-27.67	-1961.0	122.5 ^b
$\log K_{s0}$ (GdPO ₄)	307.67	0.0357	-1.214E+04	-123.01	0.992	-26.81	-1953.2	124.6 ^b

^a Ushakov et al. (2001), oxide melt calorimetry.

used together, reproduce the solubility values reported in the present study.

6.2. Parameter optimization

For CePO₄, GdPO₄, and SmPO₄, reconciling calorimetric and solubility data requires the use of an optimization method to simultaneously modify the standard thermodynamic properties of the aqueous species and/or of the minerals and recalculate the solubility of the REE phosphates. Using the global optimization algorithm GEMSFITS (Miron et al., 2015), which is combined with the GEMS3K Gibbs energy minimization code (Kulik et al., 2013), it is possible to adjust the standard Gibbs energy of the REE aqueous species at 298.15 K and 1 bar, while recalculating their activities and speciation in the experiments.

The approach taken was to minimize the difference between the total measured REE and P concentrations, the pH of the experiments (Table A1) and their calculated values, while simultaneously assuring that the system is saturated with the REE phosphates during the optimization. Without changing the entropy and heat capacity of REE phosphates (Table 2) and aqueous species, as well as using the reported HKF parameters for REE aqueous species (Supcrt92 database, Table A3), it was possible to resolve the discrepancies by either adjusting the standard molal Gibbs energy of REE³⁺ and REEOH²⁺ or by adjusting the Gibbs energy of REEPO₄(s) and REEOH²⁺.

In the first mode (I), the lowest residuals (i.e. differences between experimental and calculated values) were obtained by optimizing simultaneously the standard Gibbs energy of REE³⁺ and REEOH²⁺ (i.e., the two major species at the experimental conditions). For this optimization, the standard thermodynamic properties of the REE phosphates

(enthalpy, entropy and heat capacity) were fixed from available calorimetric measurements using the values in Table 2. In the second mode (II), identical residuals were obtained by simultaneously adjusting the standard Gibbs energy of REEPO₄(s) and REEOH²⁺, while fixing the entropy and heat capacity of the REE phosphates from calorimetric measurements (Table 2) and the thermodynamic properties for the REE³⁺ ion from the Supert92 database (Table A3). The properties of other aqueous species were fixed. The properties of the other REE hydroxyl species, including REEO⁺, REEO₂H⁰, REEO₂ (i.e., the corresponding hydrated species are REE(OH)₂⁺, REE(OH)₃⁰, REE (OH)₄, were constrained by their association constants from the data of Haas et al. (1995) to maintain internal consistency with the new optimized data. The results of these optimizations (i.e., modes I and II) are listed in Table 5.

In both cases, just adjusting the standard Gibbs energy of REEPO₄(s) or of the REE³⁺ ion alone was not enough to mitigate the discrepancies with the measured experimental values, as seen in Fig. 6. For example, comparison of the measured solubility data for CePO₄ with the calculated solubility using the Supert92 database shows that the concentration of the Ce³⁺ ion decreases with T, where a shift up or down (change in the Gibbs energy) is not sufficient to minimize the differences between experiments and theoretical predictions. Only by optimizing the Gibbs energy of the CeOH²⁺ species, which displays an increase in concentration with temperature, resulted in a much better agreement with the experimental data (compare the blue and gray dotted lines in Fig. 6). The same behavior was observed for the Gd and Sm phosphates, where the discrepancies could only be resolved by optimizing simultaneously the standard Gibbs energy for the REEOH²⁺ species and either the Gibbs energy of the REE phosphates or the REE³⁺ ion.

^b Thiriet et al. (2004, 2005), adiabatic calorimetry.

^c Enthalpy of formation of REE phosphates recalculated from fitted standard enthalpy of reaction $(\Delta_r H^0_{Tr,Pr})$ using Reaction (3) and standard enthalpies of formation $(\Delta_J H^0_{Tr,Pr})$ of -1277.9 kJ/mol for PO_3^{4-} , -700.4 kJ/mol for Ce^{3+} , -691.2 kJ/mol for Sm^{3+} and -687.0 kJ/mol for Gd^{3+} from Shock and Helgeson (1988) and Shock et al. (1997).

^d Absolute entropy of REE phosphates recalculated from fitted standard entropy of reaction ($\Delta_r S_{Tr,Pr}^0$) data using Reaction (3) and standard entropies (S^0) of PO₃⁴, Ce³⁺, Sm³⁺ and Gd³⁺ listed in Table A3.

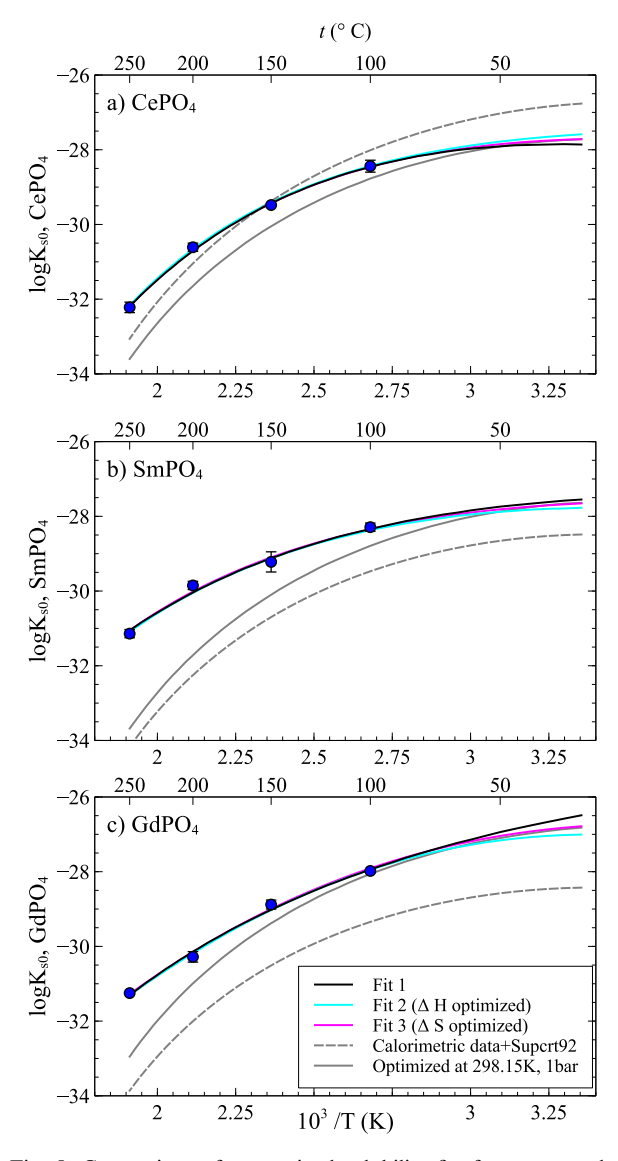


Fig. 5. Comparison of constrained solubility fits from our study (Table 4; Fits 2 and 3) with combined Supert92 data for aqueous species (Shock and Helgeson, 1988; Shock et al., 1997) with calorimetric data of the minerals in Table 2. Optimized fits at 298.15 K (grey solid line), correspond to Supert92 data for aqueous species combined with the calorimetric data of Table 2 updated with the mineral enthalpy data according to Table 4.

The standard state properties for the REE aqueous species listed in Table A3, can now be combined with their optimized $\Delta_J G_{Tr,Pr}^0$ values listed in Table 5. These optimized values allow for the reconciliation of discrepancies between solubility measurements and combined calorimetric mineral data by revising the Supert92 values for aqueous REE species. It is important to note that the accuracy of the optimized data for the REE hydroxyl species will need to be verified in future potentiometric studies and solubility experiments at varying pH, and as such, these values should be regarded as provisional. Further, to maintain consistency with experimental data available for the REE chlo-

ride, fluoride complexes and other REE complexes relying on the properties of REE³⁺ from the Supcrt92 dataset, at this stage it is recommended to use the optimization that does not involve the free REE³⁺ ion (mode II). Hence, the calorimetric data of the REE phosphates in Table 2 (i.e., $S_{298.15~K}^{\circ}$, V_m and Cp° function) can be used with the optimized standard Gibbs energy of these solids at 298.15 K and 1 bar (-1850.6 ± 0.5 kJ/mol for CePO₄; -1842.5 ± 3.2 kJ/mol for SmPO₄; -1835.5 ± 1.5 kJ/mol for GdPO₄). Updated solubility constants based on these optimized thermodynamic properties are found in Table 6.

6.3. Speciation of REE³⁺ and hydroxyl species

Using the optimized thermodynamic properties for REE species generated in this study (Table 5), it is possible to first delineate their effects on the overall solubility of Ce, Sm and Gd without including other ligands. Experimental data determining the stability of aqueous hydroxyl complexes under hydrothermal conditions are scarce. One study has determined the hydrolysis constants for Nd at temperatures up to 290 °C (Wood et al., 2002), and demonstrated an increased importance of Nd³⁺ over Nd(OH)²⁺, in comparison to the theoretical predictions of Haas et al. (1995). Another study by Pourtier and Devidal (2010) determined the solubility of monazite-(Nd) from 300 to 800 °C at 2 MPa. In contrast to the experimental data of Wood et al. (2002), their solubility study concluded that at 300 ° C, a stronger contribution of Nd(OH)²⁺ over Nd³⁺ can be expected in the low pH range, which agrees better with the predictions of Haas et al. (1995). However, their data also showed better agreement with the experimental data of Wood et al. (2002) at pH values of 3 to 6. These observations highlight the uncertainty of the thermodynamic properties of these two species at elevated temperatures.

We have constructed pH vs. log activity diagrams (Fig. 7) to display the effects of the correction of the standard properties for aqueous REE species based on our solubility experiments. The data for Ce, Sm and Gd aqueous species all display similar trends. The optimized thermodynamic data indicate that at 250 °C, the REEOH²⁺ complex becomes dominant over REE³⁺ at pH values <4, whereas the predicted data from Supcrt92 would underestimate the formation of this complex (Shock and Helgeson, 1988; Haas et al., 1995; Shock et al., 1997). The REE hydroxyl species that are stable at pH values of >4 are similar in the optimized calculations but with overall higher activities. These speciation calculations are somewhat similar to the study of Pourtier and Devidal (2010) at 300 °C, where the dominant REE species at low pH was Nd $(OH)^{2+}$, followed by $Nd(OH)_{2}^{+}$ at pH values between ~ 3 and 7, and Nd(OH) $_3^0$ at pH > 7. Note that the independent optimization of REE(OH) $_{2}^{+}$, REE(OH) $_{3}^{0}$, and REE(OH) $_{4}^{-}$, was not possible in our study, since our solubility experiments have been carried out at pH values of 2, where either the REE³⁺ or REE(OH)²⁺ species are dominant depending on the temperature. This highlights again the need for potentiometric studies as a function of temperature and pH to constrain the properties of the other hydroxyl species in future studies.

Table 5
Provisional revised values of the standard molal Gibbs energy of aqueous REE species from Supert92 optimized using GEMSFITS, which permit reproducing the measured solubilities of this study. Optimizations include mode I (optimization of REE³⁺ and REEOH²⁺) and mode II (optimization of REEOH²⁺ and REEPO₄(s)).

		Mode I			Mode II		
Species	$\Delta_{\rm f}G^0_{298.15,\ 1bar}$ (Supcrt92) J/mol	$\Delta_{\rm f}G_{298.15,\ 1bar}^0$ (this study) J/mol	σ	Optimization	$\Delta_{\rm f}G_{298.15,\ 1bar}^0$ (this study) J/mol	σ	Optimization
Ce ³⁺	-676,134	-673,056	480	Optimized	_		Fixed
CeOH ²⁺	-865,251	-879,975	601	Optimized	-883,051	882	Optimized
CeO^+	-819,646	-834,370	_	^a Constrained	-837,446	_	^a Constrained
CeO_2^-	-929,266	-943,990	_	^b Constrained	-947,066	_	^b Constrained
CeO_2H^0	-1,001,231	-1,015,955	_	^c Constrained	-1,019,031	_	^c Constrained
Sm ³⁺	-665,674	-669,941	5207	Optimized	_		Fixed
$SmOH^{2+}$	-857,302	-888,228	1092	Optimized	-883,868	3485	Optimized
SmO^+	-808,767	-839,693	_	^a Constrained	-835,333	_	^a Constrained
SmO_2^-	-940,145	-971,071	_	^b Constrained	-966,711	_	^b Constrained
SmO_2H^0	-992,026	-1,022,952	_	Constrained	-1,018,592	_	^c Constrained
Gd^{3+}	-663,582	-672,515	1337	Optimized	_		Fixed
$GdOH^{2+}$	-855,628	-884,499	745	Optimized	-875,566	2061	Optimized
GdO^+	-807,512	-836,383	_	^a Constrained	-827,450	_	^a Constrained
GdO_2^-	-941,400	-970,271	_	^b Constrained	-961,338	_	^b Constrained
GdO_2H^0	-993,700	-1,022,571	_	^c Constrained	-1,013,638	_	^c Constrained

Note the convention used for the REE hydroxyl species in the Supcrt92 dataset, which can be converted to the hydrated species notation listed in Table 1, where REEO⁺ + $H_2O = REE(OH)_2^+$, $REEO_2^- + 2H_2O = REE(OH)_4^-$, and $REEO_2H^0 + H_2O = REE(OH)_3^0$. The standard deviation (σ) in the optimizations was calculated from 200 Monte Carlo simulations. Association constants were fixed by the original fits by Haas et al. (1995) according to the reactions:

7. IMPLICATIONS FOR MONAZITE SOLUBILITY AND REE MOBILITY IN THE CRUST

7.1. Compositions of natural monazite

Natural monazite forms a highly varied series of solid solution compositions between the different LREE (i.e., La, Ce, Nd, Pr, Eu, and Gd) (Boatner, 2002). The principal REE in monazite is Ce with lesser amounts of the remaining REE, coupled with the incorporation of additional elements including Th, U, Si and Ca. Metasomatic alteration from a variety of fluids has been recognized as an important mechanism with respect to the stability and compositions of monazite-(Ce) in high-grade metamorphic rocks (Mair et al., 2017; Tropper et al., 2011, 2013), which also has implications with regard to its use in geochronology as a recorder of high-grade metasomatic events (Poitrasson et al., 1996; Harlov, 2011; Harlov et al., 2011; Williams et al., 2011; Grand'homme et al., 2016). Both pressure and temperature also play a role, but to a lesser extent due to the slow rates of element diffusion measured in monazite (Cherniak et al., 2004a, 2004b). Due to its very low solubility in low temperature fluids, monazite is also known to control the mobility of the REE, and in many cases may control fractionation of the REE measured in other hydrothermal minerals such as calcite (Debruyne et al.,

2016; Perry and Gysi, 2018). In addition, the kinetics of dissolution may also play a role in low temperature systems, where pH affects the dissolution rates of monazite (Oelkers and Poitrasson, 2002). Rhadophane has been reported in low temperature mineral assemblages associated to supergene weathering and secondary REE enrichment (Hutchinson, 2016; Andersen et al., 2017). Rhabdophane may also play a significant role in controlling the chemistry of seawater and the mobility of the REE associated to weathering and soil formation (Jonasson et al., 1985; Byrne and Kim, 1993).

Monazite occurs in many REE mineral deposits including carbonatites and associated alkaline intrusives (Smith et al., 2000; Wall et al., 2008; Moore et al., 2015; Trofanenko et al., 2016), and iron oxide-apatite (IOA) deposits (Harlov et al., 2002; Harlov et al., 2016; Hofstra et al., 2016; Jonsson et al., 2016). Fig. 8 shows the compositional variations of natural monazite associated with REE deposits. Chondrite normalized REE profiles (Fig. 8a) display large variations between different mineral deposits, with monazite from Lofdal being enriched in the heavy REE in comparison to Bayan Obo and Wicheeda. To illustrate the importance of studying endmember REE phosphate stabilities, such as CePO₄, SmPO₄ and GdPO₄, we plotted ratios of Ce/Sm vs. Ce/Gd (Fig. 8b). These ratios vary orders of magnitude between monazite compositions

^a $REEOH^{2+} = H^+ + REEO^+$.

^b REEOH²⁺ + $H_2O = 3H^+ + REEO_2^-$.

^c REEOH²⁺ + H_2^{-} O = $2H^+$ + REEO₂ H^0 .

d The optimized standard Gibbs energies for the REEPO₄(s) at 298.15 K and 1 bar (mode II) are: -1850.6 ± 0.5 kJ/mol for CePO₄; -1842.5 ± 3.2 kJ/mol for SmPO₄; -1835.5 ± 1.5 kJ/mol for GdPO₄. These values are internally consistent with entropy and Cp data of Table 2.

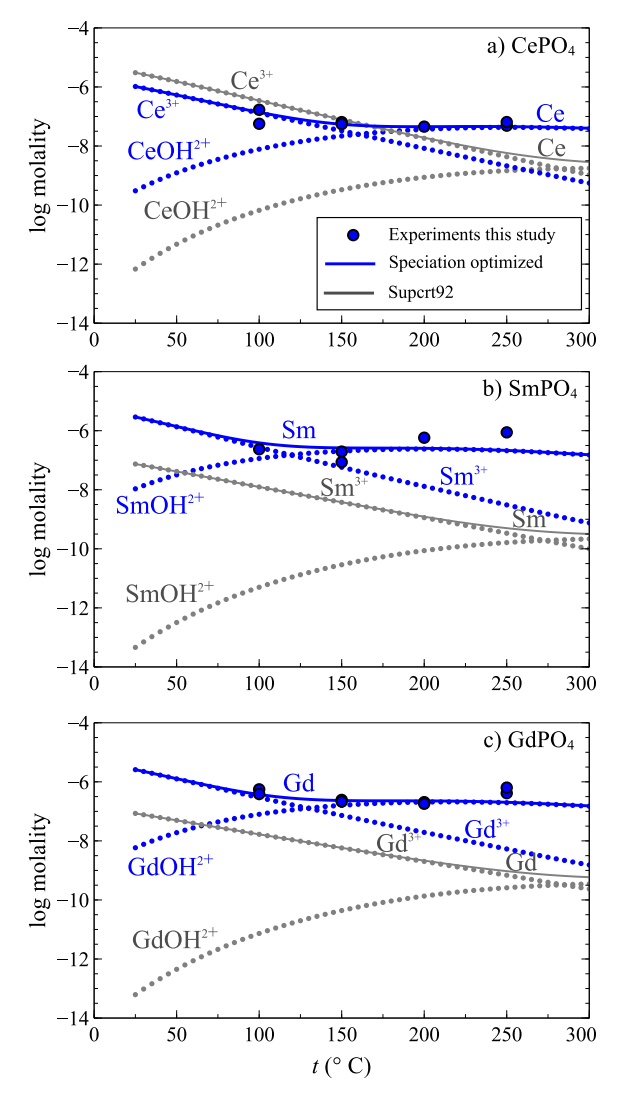


Fig. 6. Calculated solubility of (a) CePO₄, (b) SmPO₄, and (c) GdPO₄ as a function of temperature showing the total dissolved molalities of REE (solid lines) and major aqueous REE species (dotted lines) at the experimental conditions. Thermodynamic data for the optimized aqueous REE species from Table 5 were used to calculate the optimized speciation and are compared to calculations using the values from Supert92 (Haas et al., 1995; Shock and Helgeson, 1988; Shock et al., 1997). Note that an increase in the stability of REEOH²⁺ is necessary to reproduce the higher observed REE solubility at elevated temperature.

Table 6 Updated values of the logarithm of the solubility product ($\log K_{s0}$) of REE phosphates consistent with the optimized values for aqueous REE species listed in Table 5 and the calorimetric values listed in Table 2.

t (°C)	$\log K_{\rm s0}~({\rm CePO_4})$	$\log K_{\rm s0} ({\rm SmPO_4})$	$\log K_{\rm s0} ({\rm GdPO_4})$
100	-28.4	-28.8	-28.1
150	-29.8	-30.1	-29.4
200	-31.4	-31.7	-31.0
250	-33.4	-33.7	-33.0

from different deposits as well as within the deposits themselves. The ore-forming processes involve deposition of monazite from hydrothermal fluids enriched in incompatible elements and/or from interaction of these fluids with the host rocks and mineral replacement reactions, for example with apatite (Smith et al., 2000; Wall et al., 2008; Harlov, 2011; Harlov et al., 2002, 2016; Jonsson et al., 2016; Trofanenko et al., 2016). These magmatic fluids are enriched in Cl and other potential ligands such as F and CO₂ that affect the solubility of monazite and other REE minerals due to the formation of complex with the REE (Migdisov et al., 2009). However, the prediction of the exact changes in the composition of monazite solid solutions associated with these fluid-rock interaction processes as a function of varying P-T-x conditions remains to be determined. These variations in the REE compositions of natural monazite, yield promising signatures that may be used to constrain the physico-chemical conditions of metasomatism in the crust. To be able to do such predictions, better constraints on the stability of the monazite solid solutions and the REE aqueous speciation are needed.

7.2. The link between REE ionic radii, monazite solubility and natural compositions

One of the interesting aspects of comparing a wide variety of natural monazite compositions (Fig. 8a), is that the chondrite normalized REE profiles display two groups for the LREE. One group displays limited fractionation and includes La, Ce, Pr, and Nd, whereas the other group displays a strong fractionation and includes Sm. Eu. and Gd. These variations could be explained by the incorporation of REE with varying ionic radii into the monazite structure. For example, this behavior is reflected in the varying molar volumes of the different monazite endmembers (Ni et al., 1995), mechanical properties (Wilkinson et al., 2017), and also by local lattice strain and possible reordering resulting from the substitution of REE with difference in ionic radii in binary solid solutions of La-Eu and La-Gd phosphates (Geisler et al., 2016; Huittinen et al., 2017). This behavior is also reflected in measured excess enthalpy of mixing in binary solid solutions (Popa et al., 2007; Neumeier et al., 2017). Comparison of our optimized solubility constants for CePO₄, SmPO₄, and GdPO₄ (Fig. 9) with the ones for NdPO₄ from Poitrasson et al. (2004), indicates similarly to the natural monazite compositions, two groups of REE with systematic behavior depending on their ionic radii. One group corresponds to CePO₄ and NdPO₄, where the Nd endmember with the smaller ionic radius displays a higher solubility. The other group corresponds to SmPO₄ and GdPO₄, where again the Gd endmember with the smaller ionic radius displays a higher solubility, and hence, a lower stability. To better understand the exact nature of this behavior, i.e. whether it is an intrinsic property of the solid due to lattice strain or related to the hydration of ions in aqueous solutions, will require additional solubility data for the other REE phosphates in this temperature range.

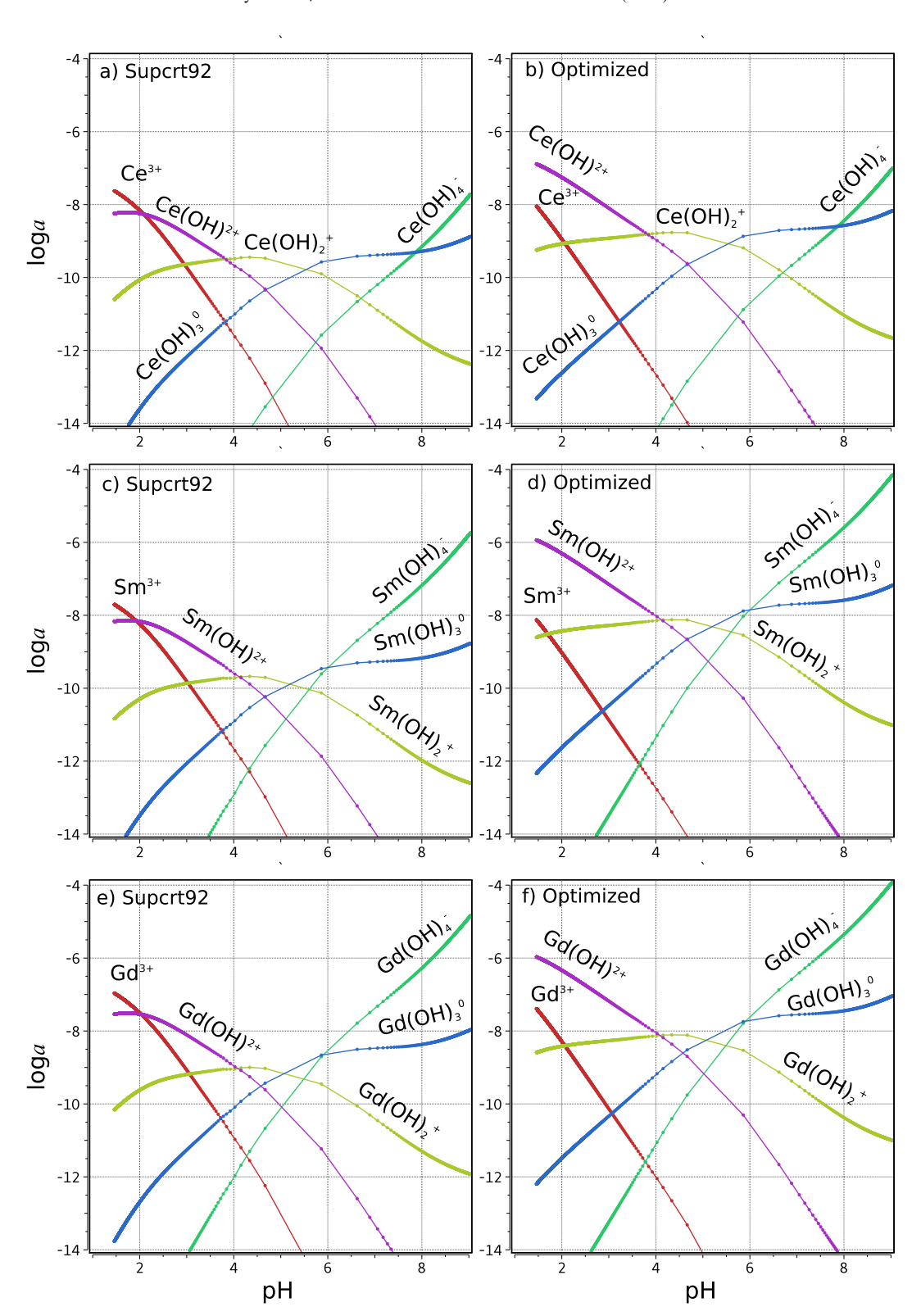


Fig. 7. Speciation diagram at 250 °C and *swvp* showing the logarithm of the activity of aqueous REE species vs. pH for solutions in equilibrium with (a-b) CePO₄, (c-d) SmPO₄ and (e-f) GdPO₄. Thermodynamic properties for aqueous REE species used in the calculations are from Supert92 (Shock and Helgeson, 1988; Haas et al., 1995; Shock et al., 1997) and the optimized values listed in Table 5.

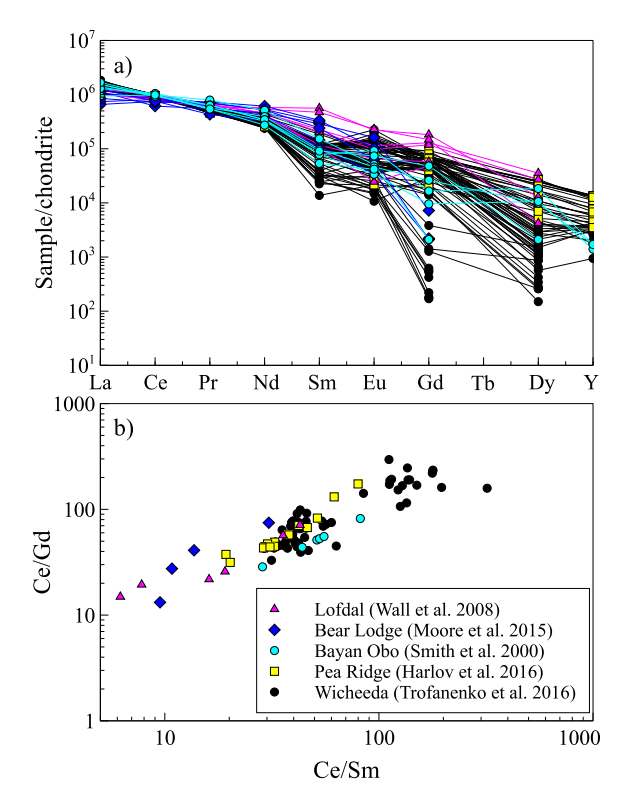


Fig. 8. (a) Rare earth element profiles of samples (ppm) normalized to chondrite (McDonough and Sun, 1995), and (b) molar ratios of Ce/Sm vs. Ce/Gd, showing the compositional variation of REE in natural monazite. Selected REE deposits include carbonatites (Lofdal in Namibia, Bear Lodge in Wyoming, Bayan Obo in China, and Wicheeda in British Columbia) and iron-oxide-apatite (Pea Ridge) deposits.

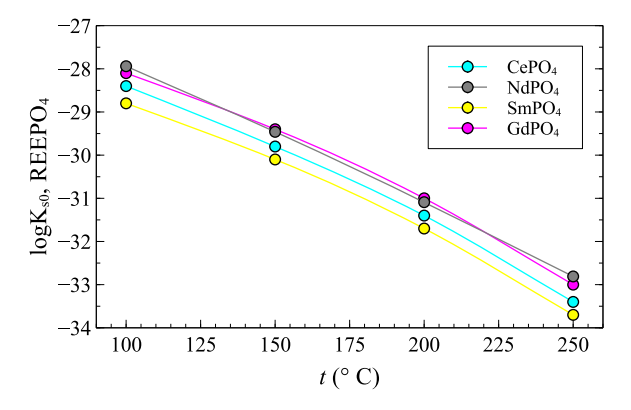


Fig. 9. Comparison of the optimized solubility products ($\log K_{s0}$) for CePO₄, SmPO₄, and GdPO₄ from this study and NdPO₄ from the study of Poitrasson et al. (2004). Note that the solubility behavior of the LREE (i.e. increasing with decreasing ionic radii) can be categorized into two groups, similarily to the composition of REE in natural monazite (Fig. 8a), where Ce and Nd are less fractionated, and Sm and Gd are more fractionated.

7.3. The role of Cl, F and P for REE mobility in fluids

In low pH experimental studies, the REE phosphates display very low solubilities in the ppb to ppt range at 25

to ~400 °C (Poitrasson et al., 2004; Cetiner et al., 2005; Gysi et al., 2015). This is mainly observed for experimental conditions where only REE³⁺ and hydroxyl complexes are dominant even at higher pressures (Louvel et al., 2015). In REE mineral deposits, however, additional ligands have been determined to be important for increasing the solubility of REE-bearing minerals, including Cl⁻, F⁻, SO₄²⁻, and CO_3^{2-} . The presence of these ligands has been determined based on fluid inclusion analysis and the occurrence of hydrothermal fluorite and calcite veins. These observations have been made in: peralkaline granititic systems such as Strange Lake in Canada (Salvi and Williams-Jones, 1990; Gysi and Williams-Jones, 2013; Vasyukova et al., 2016; Vasyukova and Williams-Jones, 2018), hydrothermal breccia and vein deposits such as Gallinas in New Mexico and Snowbird in Montana (Williams-Jones et al., 2000; Gagnon et al., 2003; Samson et al., 2004), IOA deposits such as Pea Ridge (Hofstra et al., 2016), and carbonatites such as Bayan Obo in China (Smith et al., 2000). In the recent numerical modeling study by Migdisov and Williams-Jones (2014), based on available experimental data up to \sim 350 °C (Migdisov et al., 2009), it was posited that in natural systems, Cl plays a major role in the transport of REE at low pH, whereas F plays a role as depositional ligand under mildly acidic conditions to higher pH. This is related to the low solubility of REE fluorides with increased pH, which limits the conditions at which F can play an important role as a ligand in REE transport. The REE concentrations in Cl-bearing solutions can increase to ppm and even wt.% concentrations (Gammons et al., 1996; Migdisov and Williams-Jones, 2014; Louvel et al., 2015). The REE fluorocarbonates display a very low solubility (Gysi and Williams-Jones, 2015), therefore possibly limiting the role of carbonate complexes for REE mobilization in hydrothermal fluids. The same applies to phosphorus, where the low solubility of REE phosphates may limit the transport of REE, and P may be expected to behave as a depositional ligand similar to F.

However, experiments at 800 °C and 1000 MPa have shown that addition of NaF and NaCl increased considerably the solubility of CePO₄ and YPO₄, and addition of these salts to the fluids allow the effective fractionation of Ce from Y (Mair et al., 2017; Tropper et al., 2011, 2013). This was also observed in the experimental study by Zhou et al. (2016) at 800 °C and 500 MPa where addition of KCl increased the fractionation of LREE and HREE in synthetic fluid inclusions, and addition of Na to F- and CO₂-bearing solutions increased the solubility of the REE phosphates. This indicates the need for additional experimental data for investigating the role of P, F, and CO₂ over a wider P-T and pH range (Tsay et al., 2014; Louvel et al., 2015) to better assess their role for REE transport in natural systems.

7.4. Model of the hydrothermal solubility of an ideal monazite solid solution

The solubility of an ideal monazite solid solution was simulated as a function of temperature and salinity to test the implications of our updated thermodynamic data on

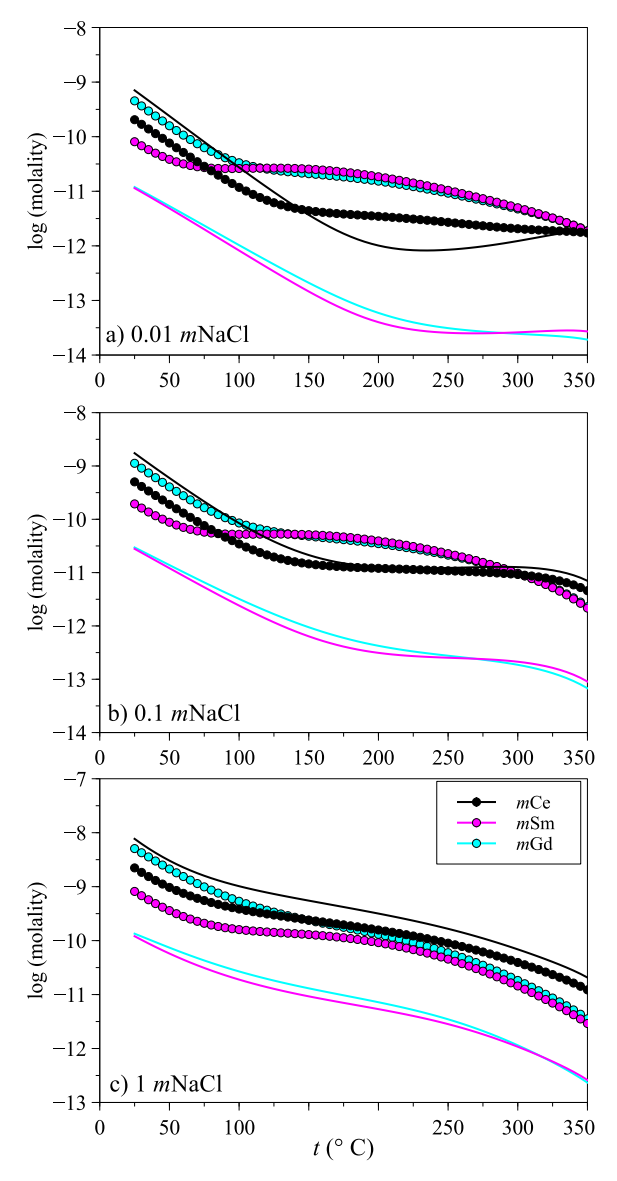


Fig. 10. Simulated solubility of Ce, Sm and Gd (molality) as a function of temperature at 500 bar in equilibrium with REEPO₄ solid solutions using GEM-Selektor. The initial solution composition was 200 ppm REE, 200 ppm P and 0.001 m HCl, with salinities of (a) 0.01 m NaCl, (b) 0.1 m NaCl and (c) 1 m NaCl. The model assumes an ideal solid solution model between CePO₄, SmPO₄ and GdPO₄ endmembers. The lines correspond to the model using the thermodynamic properties for aqueous REE³⁺ and hydroxyl complexes from Supcrt92 (Shock and Helgeson, 1988; Haas et al., 1995; Shock et al., 1997) and Table 2 for minerals, and the symbols correspond to the model using the properties optimized in this study (Table 5; Mode II). Thermodynamic data for the REE chloride complexes were taken from the experimental study of Migdisov et al. (2009).

the solubility of Ce, Gd and Sm (Fig. 10). These simulations include the REE chloride species determined in the experiments by Migdisov et al. (2009) to study the effects of mineral solubilities controlled by REE hydroxyl species vs. chloride species. Using the data presented in this study, the total molalities of Ce is generally lower than Sm and

Gd, whereas the molality of Ce is higher than Sm and Gd by several orders of magnitude using the aqueous species thermodynamic data from the Super92 dataset (Shock and Helgeson, 1988; Haas et al., 1995; Shock et al., 1997). Considering that in natural systems monazite-(Ce) is the most common light REE phosphate, the simulated predictions using the data obtained in this study are more consistent with observations of natural systems. Consequently, CePO₄ would be expected to be the least soluble. This is in line with the numerical simulations with 0.01 mNaCl at temperatures above 50 °C (Fig. 10a). Increasing the amount of NaCl to 0.1 m and 1 m (Fig. 10b and c), shifts the total molality of the dissolved Ce, Sm, and Gd to higher values, and overall increases the amount of dissolved Ce, which highlights the importance of Cl-rich fluids for the hydrothermal mobilization of REE (Williams-Jones et al., 2012; Gysi and Williams-Jones, 2013; Migdisov and Williams-Jones, 2014; Perry and Gysi, 2018). These simulations demonstrate that the updated data for aqueous species yields overall higher calculated solubilities than previously predicted, especially for the monazite-(Gd)and -(Sm) endmembers. This will directly affect the calculation of solid solution compositions, i.e. the lower solubility of CePO₄ and increased solubilities of SmPO₄ and GdPO₄ will result in a solid solution composition that is more Ce-rich, in line with natural observations. Better constraint of the stability and composition of monazite solid solutions in natural systems, will require a detailed revision of the thermodynamic data for all the REE phosphate endmembers and their aqueous species. One may be inclined to assume ideal mixing between the REE phosphate endmembers, due to similarities between the ionic radii of the different REE. However, recent studies have demonstrated that binary solid solutions between REE phosphate endmembers are characterized by non-ideal mixing determined by experiments and from ab initio modeling (Popa et al., 2007; Li et al., 2014; Geisler et al., 2016; Gysi et al., 2016; Hirsch et al., 2017).

8. CONCLUSION AND OUTLOOK

We have measured the solubility of the monazite endmembers CePO₄, SmPO₄, and GdPO₄ in aqueous HClO₄-H₃PO₄ solutions at temperatures from 100 to 250 °C. Combining calorimetric data available for REE phosphates with the aqueous species from Supert92 (Shock and Helgeson, 1988; Haas et al., 1995; Shock et al., 1997) commonly used to calculate the stability of REE complexes and minerals, has demonstrated large discrepancies with our solubility measurements. In a previous study (Gysi et al., 2015) we showed how to optimize the enthalpy for the REE phosphates, whereas in this study we propose a provisional revised dataset of standard thermodynamic properties for aqueous REE species until further experimental measurements become available. This permitted us to reconcile solubility measurements with available calorimetric data for the minerals. The compositional changes of monazite solid solutions in equilibrium with hydrothermal fluids is complex, as it requires a detailed knowledge of thermodynamic properties of the mixing properties of their solid solutions, and the stability of aqueous complexes. The present study is a first step for improving our prediction capabilities of monazite compositions in equilibrium with crustal fluids, but future studies will need careful determination of the properties of binary solid solutions to use monazite compositions as possible signatures of crustal metasomatism. These and future data will be implemented in the MINES thermodynamic database (Gysi, 2017), together with the recently developed internally consistent datasets for rock forming minerals and major aqueous species (Miron et al., 2016; Miron et al., 2017). These advances will permit the more accurate simulation of the stability and composition of REE phosphates in complex natural systems at various physico-chemical conditions.

ACKNOWLEDGMENTS

This project was supported by the National Science Foundation to APG (NSF grant EAR-1649656). We would like to thank Chris Van Hoozen, Katie Challis and James Ranville for help on ICP-MS analysis, and Katharina Pfaff for SEM analysis. We are also grateful for the useful comments by Artas Migdisov and two anonymous reviewers, and would like to thank Associate Editor Rosemary Hickey-Vargas for handling this manuscript.

APPENDIX A

See Tables A1-A3.

Table A1
Composition of quenched experimental solutions (mol/kg) from solubility experiments performed at saturated water vapor pressure (*swvp*) and calculated logarithm of activities for aqueous species used for retrieving the solubility product from Eq. (11) and data in Table A2.

Type	Time (days)	t (°C)	pН	$mClO_4^-$	mP	mREE	$log aH_3PO_4^0$	$log a H_2 PO_4^-$	$log a HPO_4^{2-}$	$log a PO_4^{3-}$	logaREE ³⁺	logaREEOH ²⁺
CePO ₄	1	100	2.015	1.09E-02	2.13E-05	3.44E-08	-4.790	-5.345	-10.623	-20.748	-7.961	-11.402
	2	100	2.015	1.09E-02	2.03E-05	2.75E-08	-4.812	-5.366	-10.644	-20.769	-8.057	-11.499
	3	100	2.015	1.09E-02	1.95E-05	1.08E-07	-4.830	-5.384	-10.662	-20.787	-7.466	-10.907
	3	100	2.015	1.09E-02	2.05E-05	3.90E-08	-4.815	-5.370	-10.648	-20.773	-7.907	-11.348
	4	100	2.015	1.09E-02	2.04E-05	6.13E-08	-4.811	-5.365	-10.643	-20.768	-7.710	-11.151
	5	100	2.015	1.09E-02	2.10E-05	8.19E-08	-4.796	-5.351	-10.628	-20.754	-7.585	-11.026
	5	100	2.015	1.09E-02	2.05E-05	1.21E-07	-4.808	-5.363	-10.641	-20.766	-7.414	-10.855
	14	100	2.015	1.09E-02	1.03E-05	1.69E-07	-5.105	-5.659	-10.937	-21.062	-7.269	-10.710
	21	100	2.015	1.09E-02	1.83E-05	5.67E-08	-4.856	-5.411	-10.688	-20.814	-7.744	-11.185
	14	150	2.023	1.09E-02	1.12E-05	5.53E-08	-5.011	-5.884	-11.392	-21.661	-7.825	-9.882
	14	150	2.023	1.09E-02	9.78E-06	6.46E-08	-5.072	-5.945	-11.452	-21.722	-7.758	-9.815
	14	200	2.033	1.09E-02	1.17E-05	4.54E-08	-4.960	-6.184	-12.021	-22.586	-8.022	-8.977
	14	250	2.048	1.09E-02	1.06E-05	4.89E-08	-4.987	-6.620	-12.895	-23.892	-8.226	-8.260
	14	250	2.048	1.09E-02	5.08E - 06	6.47E - 08	-5.306	-6.939	-13.213	-24.211	-8.103	-8.138
$SmPO_4$	14	100	2.015	1.09E-02	8.11E-06	2.36E-07	-5.210	-5.764	-11.042	-21.167	-7.124	-10.245
	14	150	2.023	1.09E-02	8.70E - 06	8.62E - 08	-5.123	-5.996	-11.503	-21.773	-7.635	-9.433
	14	150	2.023	1.09E - 02	9.11E-06	1.96E-07	-5.103	-5.976	-11.483	-21.753	-7.277	-9.075
	14	200	2.033	1.09E-02	5.47E-06	5.79E-07	-5.292	-6.515	-12.353	-22.917	-6.928	-7.680
	14	250	2.048	1.09E-02	6.20E - 06	8.79E-07	-5.219	-6.853	-13.127	-24.124	-7.015	-6.894
$GdPO_4$	14	100	2.015	1.09E-02	9.39E-06	3.87E-07	-5.147	-5.700	-10.978	-21.103	-6.910	-9.990
	14	100	2.015	1.09E-02	7.72E-06	5.57E-07	-5.232	-5.786	-11.064	-21.188	-6.752	-9.832
	14	150	2.023	1.09E - 02	1.25E-05	2.44E-07	-4.967	-5.839	-11.347	-21.616	-7.183	-8.987
	14	150	2.023	1.09E-02	9.69E - 06	2.14E-07	-5.076	-5.949	-11.456	-21.726	-7.240	-9.044
	14	200	2.033	1.09E-02	4.47E-06	2.05E-07	-5.379	-6.603	-12.441	-23.005	-7.376	-8.183
	14	200	2.033	1.09E-02	8.02E - 06	1.81E-07	-5.125	-6.349	-12.187	-22.751	-7.429	-8.236
	14	250	2.048	1.09E-02	9.58E-06	4.14E-07	-5.031	-6.664	-12.938	-23.936	-7.309	-7.296
	14	250	2.048	1.09E-02	6.21E-06	6.36E - 07	-5.219	-6.852	-13.126	-24.123	-7.123	-7.110

Table A2
Logarithm of the ionization constants for orthophosphoric acid using the data of Shock and Helgeson (1988), Shock et al. (1989) and Shock et al. (1997).

t (°C)	$\log K$			
	100	150	200	250
Reactions				
$H_3PO_4^0 = H^+ + H_2PO_4^- (K_1)$	-2.57	-2.90	-3.26	-3.68
$H_2PO_4^- = H^+ + HPO_4^{2-}(K_2)$	-7.26	-7.53	-7.87	-8.32
$HPO_4^{2-} = H^+ + PO_4^{3-} (K_3)$	-12.14	-12.29	-12.60	-13.05

Standard state properties at 298.15 K and 1 bar, and HKF parameters of aqueous REE species from Shock and Helgeson (1988), Haas et al. (1995) and Shock et al. (1997). The optimized standard molal Gibbs energies are listed in Table

Species	\mathbf{S}_0	පි	οΛ	al	a2	а3	a4	cl	c5	0w
•	$\mathrm{J} \ \mathrm{mol}^{-1} \mathrm{K}^{-1}$	$\mathrm{J}\mathrm{mol}^{-1}\mathrm{K}^{-1}$	J/bar	$cal bar^{-1} mol^{-1}$	$cal mol^{-1}$	$cal K bar^{-1} mol^{-1}$	$cal K mol^{-1}$	$cal mol^{-1} K^{-1}$	$cal K mol^{-1}$	$cal mol^{-1}$
Ce ³⁺	-205.02	-198.58	-4.483	-0.34833	-1627.89	12.1302	-21,059	-0.355	-127,510	232,650
CeOH^{2+}	-11.30	-142.20	0.416	0.27525	-106.06	6.1673	-27,351	-3.684	-99,807	110,000
CeO^+	56.07	-318.25	0.689	0.28409	-84.3	6.0772	-27,441	-35.2162	-185,361	34,910
CeO_2^-	161.50	-477.01	2.108	0.50465	454.18	3.9626	-29,667	-51.0768	-262,767	104,490
${ m CeO}_2{ m H}^0$	202.92	-563.18	2.381	0.50117	445.82	3.9917	-29,632	-72.9937	-304,525	-3,000
Sm^{3+}	-212.13	-180.18	-4.270	-0.32065	-1561.08	11.8857	-21,337	1.9385	-118,548	229,550
SmOH^{2+}	-20.50	-131.73	0.376	0.27076	-116.76	6.2027	-27,306	-1.9523	-94,714	112,890
SmO^+	46.02	-306.52	0.658	0.28115	-91.57	6.1076	-27,410	-33.2571	-179,657	38,370
SmO_2^-	150.21	-453.08	2.037	0.49642	433.93	4.0456	-29,583	-47.3681	-251,156	108,480
$\mathrm{SmO}_2\mathrm{H}^0$	192.05	-528.2	2.396	0.49296	425.52	4.0768	-29,548	-69.5359	-292,507	-30,000
Gd^{3+}	-205.853	-149.21	-4.113	-0.29771	-1505.06	11.6656	-21,568	9095.9	-103,474	232,650
GdOH^{2+}	-12.134	-140.95	0.406	0.27389	-109.36	6.1786	-27,337	-3.5082	-99,196	110,000
GdO^{+}	54.81	-317	0.689	0.28425	-84.09	6.0801	-27,441	-34.9963	-184,750	35,390
GdO_2^-	160.25	-474.01	2.098	0.50344	451.11	3.9769	-29,654	-50.6235	-261,341	104,950
$\mathrm{GdO}_2\mathrm{H}^0$	201.67	-560.25	2.381	0.50117	445.82	3.9917	-29,632	-72.5835	-303,099	-3,000

APPENDIX B

The relation of enthalpy and heat capacity at constant pressure was determined from the Van't Hoff relation,

$$\delta \ln \mathbf{K}/\delta \mathbf{T} = \Delta_r H_T^0/(RT)^2$$

and Kirchhoff's equations,

$$[\delta \Delta H/\delta T]_P = \Delta C p$$

the symbol R is the ideal gas constant, T the temperature in Kelvin, K the equilibrium constant, in which Δ Cp is represented by the equation of Haas and Fisher (1976),

$$\Delta \text{Cp}^{\circ} = a_0 + a_1 T + a_2 T^{-2} + a_3 T^{-0.5} + a_4 T^2$$

and enthalpy by integration of the Cp equation,

$$\Delta_r H_T^0 = h_{Tr} + a_0 T + (a_1/2) T^2 - a_2/T + 2a_3 T^{0.5} + (a_4/3) T^3$$

h_{Tr} is a constant enthalpy term according to,

$$h_{Tr} = \Delta_r H_T^0 - a_0 T_r - (a_1/2) T_r^2 + a_2/T_r - 2a_3 T_r^{0.5} - (a_4/3) T_r^3$$

The integrated form of the Van't Hoff yields for a four parameter equation:

$$lnK = A_0 + A_1T + A_2/T + A_3ln(T)$$

where A0-A3 are related to A-D parameters from Eq. (13),

$$A_0 = \text{Aln}(10) = (s_{Tr} - a_0)/R$$

$$A_1 = Bln(10) = a_1/(2R)$$

$$A_2 = \operatorname{Cln}(10) = -h_{Tr}/R$$

$$A_3 = D\ln(10) = a_0/R$$

and entropy can be retrieved from the constant entropy term $(\boldsymbol{s}_{Tr}),\,$

$$s_{Tr} = \Delta_r S_{T_r}^0 - a_0 \ln T_r - a_1 T_r + a_2 / (2T_r^2) + 2a_3 T_r^{-0.5} - (a_4 / 2) T_r^2$$

i.e. a_2 , a_3 , and a_4 are not used with only four isotherms experiments.

REFERENCES

Andersen A. K., Clark J. G., Larson P. B. and Donovan J. J. (2017) REE fractionation, mineral speciation, and supergene enrichment of the Bear Lodge carbonatites, Wyoming, USA. Ore Geol. Rev. 89, 780–807.

Arinicheva Y., Gausse C., Neumeier S., Brandt F., Rozov K., Szenknect S., Dacheux N., Bosbach D. and Deissmann G. (2018) Influence of temperature on the dissolution kinetics of synthetic LaPO₄-monazite in acidic media between 50 and 130 ° C. *J. Nucl. Mater.* **509**, 488–495.

Ayers J. C. and Watson E. B. (1991) Solubility of apatite, monazite, zircon, and rutile in supercritical aqueous fluids with implications for subduction zone geochemistry. *Philos. Trans. R Soc. A Math. Phys. Eng. Sci.* 335, 365–375.

Bauer J. D., Hirsch A., Bayarjargal L., Peters L., Roth G. and Winkler B. (2016) Schottky contribution to the heat capacity of monazite type (La, Pr)PO₄ from low temperature calorimetry and fluorescence measurements. *Chem. Phys. Lett.* **654**, 97–102.

Boatner L. A. and Sales B. C. (1988) *Monazite*. Elsevier Science Publishing, United States.

- Byrne R. H. and Kim K. H. K.-H. (1993) Rare earth precipitation and coprecipitation behavior: the limiting role of PO₃ on dissolved rare earth concentrations in seawater. *Geochim. Cosmochim. Acta* 57, 519–526.
- Cetiner Z. S., Wood S. A. and Gammons C. H. (2005) The aqueous geochemistry of rare earth elements. Part XIV. The solubility of rare earth element phosphates from 23 to 150 °C. *Chem. Geol.* **217.** 147–169.
- Cherniak D. J., Watson E. B., Grove M. and Harrison T. M. (2004a) Pb diffusion in monazite: a combined RBS/SIMS study. Geochim. Cosmochim. Acta 68, 829–840.
- Cherniak D., Pyle J. and Rakovan J. (2004b) Synthesis of REE and Y phosphates by Pb-free flux methods and their utilization as standards for electron microprobe analysis and in design of monazite chemical U-Th-Pb dating protocol. *Am. Mineral.* **89**, 1533–1539.
- Cook N. J., Ciobanu C. L., O'Rielly D., Wilson R., Das K. and Wade B. (2013) Mineral chemistry of Rare Earth Element (REE) mineralization, Browns Ranges, Western Australia. *Lithos* 172–173, 192–213.
- Debruyne D., Hulsbosch N. and Muchez P. (2016) Unraveling rare earth element signatures in hydrothermal carbonate minerals using a source-sink system. *Ore Geol. Rev.* **72**, 232–252.
- Du Fou de Kerdaniel E., Clavier N., Dacheux N., Terra O. and Podor R. (2007) Actinide solubility-controlling phases during the dissolution of phosphate ceramics. *J. Nucl. Mater.* 362, 451– 458.
- Firsching F. H. and Brune S. N. (1991) Solubility products of the trivalent rare-earth phosphates. *J. Chem. Eng. Data* 36, 93–95.
- Gagnon J. E., Samson I. M., Fryer B. J. and Williams-Jones A. E. (2003) Compositional heterogeneity in fluorite and the genesis of fluorite deposits: insights from LA–ICP–MS analysis. *Can. Mineral.* 41, 365–382.
- Gammons C., Wood S. and Williams-Jones A. (1996) The aqueous geochemistry of the rare earth elements and yttrium: VI. Stability of neodymium chloride complexes from 25 to 300 °C. Cosmochim. Acta 60, 4615–4630.
- Gausse C., Szenknect S., Qin D. W., Mesbah A., Clavier N., Neumeier S., Bosbach D. and Dacheux N. (2016) Determination of the solubility of rhabdophanes LnPO₄·0.667H₂O (Ln = La to Dy). *Eur. J. Inorg. Chem.*, 4615–4630.
- Geisler T., Popa K. and Konings R. J. M. (2016) Evidence for lattice strain and non-ideal behavior in the (La_{1-x}Eu_x)PO₄ solid solution from X-ray diffraction and vibrational spectroscopy. *Front. Earth Sci.* **4**, 64.
- Grand'Homme A., Janots E., Seydoux-Guillaume A.-M., Guillaume D., Bosse V. and Magnin V. (2016) Partial resetting of the U-Th-Pb systems in experimentally altered monazite: nanoscale evidence of incomplete replacement. *Geology* 44, 4-7
- Gratz R. and Heinrich W. (1997) Monazite-xenotime thermobarometry: experimental calibration of the miscibility gap in the binary system CePO₄-YPO₄. *Am. Mineral.* **82**, 772–780.
- Gysi A. P. (2017) Numerical simulations of CO₂ sequestration in basaltic rock formations: challenges for optimizing mineral-fluid reactions. *Pure Appl. Chem.* **89**, 24–29.
- Gysi A. P. and Williams-Jones A. E. (2013) Hydrothermal mobilization of pegmatite-hosted REE and Zr at Strange Lake, Canada: a reaction path model. *Geochim. Cosmochim. Acta* 122, 324–352.
- Gysi A. P., Harlov D., Filho D. C. and Williams-Jones A. E. (2016) Experimental determination of the high temperature heat capacity of a natural xenotime-(Y) solid solution and synthetic DyPO₄ and ErPO₄ endmembers. *Thermochim. Acta* **627–629**, 61–67.

- Gysi A. P. and Williams-Jones A. E. (201) The thermodynamic properties of bastnäsite-(Ce) and parisite-(Ce). *Chem. Geol.* **392**, 87–101.
- Gysi A. P., Williams-Jones A. E. and Harlov D. (2015) The solubility of xenotime-(Y) and other HREE phosphates (DyPO₄, ErPO₄ and YbPO₄) in aqueous solutions from 100 to 250 °C and psat. *Chem. Geol.* **401**, 83–95.
- Haas J. L. J. and Fisher J. R. (1976) Simultaneous evaluation and correlation of thermodynamic data. *Am. J. Sci.* **276**, 525–545.
- Haas J. R., Shock E. L. and Sassani D. C. (1995) Rare earth elements in hydrothermal systems: Estimates of standard partial molal thermodynamic properties of aqueous complexes of the rare earth elements at high pressures and temperatures. *Geochim. Cosmochim. Acta* **59**, 4329–4350.
- Harlov D. (2011) Petrological and experimental application of REE- and actinide-bearing accessory minerals to the study of Precambrian high-grade gneiss terranes. *Geol. Soc. Am. Mem.* **207**, 13–24.
- Harlov D. E., Andersson U. B., Förster H.-J., Nystrom J. O., Dulski P. and Broman C. (2002) Apatite monazite relations in the Kiirunavaara magnetite apatite ore, northern Sweden. *Chem. Geol.* **191**, 47–72.
- Harlov D. E., Wirth R. and Hetherington C. J. (2011) Fluid-mediated partial alteration in monazite: the role of coupled dissolution-reprecipitation in element redistribution and mass transfer. Contrib. Mineral. Petrol. 162, 329–348.
- Harlov D. E., Meighan C. J., Kerr I. D. and Samson I. M. (2016) Mineralogy, chemistry, and fluid-aided evolution of the Pea Ridge Fe Oxide-(Y + REE) deposit, Southeast Missouri, USA. *Econ. Geol.* 111, 1963–1984.
- Heinrich W., Andrehs G. and Franz G. (1997) Monazite-xenotime miscibility gap thermometry. I. An empirical calibration. J. Metamorph. Geol. 15, 3–16.
- Helgeson H. C. and Kirkham D. H. (1974) Theoretical prediction of the thermodynamic behavior of aqueous electrolytes at high pressures and temperatures; II, Debye-Huckel parameters for activity coefficients and relative partial molal properties. Am. J. Sci. 274, 1199–1261.
- Helgeson H. C., Kirkham D. H. and Flowers G. C. (1981) Theoretical prediction of the thermodynamic behavior of aqueous electrolytes at high pressures and temperatures: IV. Calculation of activity coefficients, osmotic coefficients, and apparent molal and standard and relative partial molal properties to 600°. Am. J. Sci. 281, 1249–1516.
- Hetherington C. J., Harlov D. E. and Budzyń B. (2010) Experimental metasomatism of monazite and xenotime: mineral stability, REE mobility and fluid composition. *Mineral. Petrol.* 99, 165–184.
- Hirsch A., Kegler P., Alencar I., Ruiz-Fuertes J., Shelyug A., Peters L., Schreinemachers C., Neumann A., Neumeier S., Liermann H. P., Navrotsky A. and Roth G. (2017) Structural, vibrational, and thermochemical properties of the monazite-type solid solution La_{1-x}Pr_xPO₄. *J. Solid State Chem.* **245**, 82–88.
- Hofstra A. H., Meighan C. J., Song X., Samson I., Marsh E. E., Lowers H. A., Emsbo P. and Hunt A. G. (2016) Mineral thermometry and fluid inclusion studies of the Pea Ridge iron oxide-apatite-rare earth element deposit, Mesoproterozoic St. Francois Mountains Terrane, Southeast Missouri, USA. Econ. Geol. 111, 1985–2016.
- Huittinen N., Arinicheva Y., Kowalski P. M., Vinograd V. L., Neumeier S. and Bosbach D. (2017) Probing structural homogeneity of La_{1x}Gd_xPO₄ monazite-type solid solutions by combined spectroscopic and computational studies. *J. Nucl. Mater.* 486, 148–157.

- Hutchinson M. B. (2016) REE Enrichment in Weathered Carbonatite, Bull Hill: Bear Lodge Mountains, Wyoming M.Sc. thesis. Colorado School of Mines.
- Ji Y., Beridze G., Bosbach D. and Kowalski P. M. (2017) Heat capacities of xenotime-type ceramics: an accurate ab initio prediction. J. Nucl. Mater. 494, 172–181.
- Johnson J. W., Oelkers E. H. and Helgeson H. C. (1992) SUPCRT92: A software package for calculating the standard molal thermodynamic properties of minerals, gases, aqueous species, and reactions from 1 to 5000 bars and 0 to 1000 °C. Comput. Geosci. 18, 899–947.
- Jonasson R. G. G., Bancroft G. M. M. and Nesbitt H. W. W. (1985) Solubilities of some hydrous REE phosphates with implications for diagenesis and sea water concentrations. *Geochim. Cosmochim. Acta* 49, 2133–2139.
- Jonsson E., Harlov D. E., Majka J., Högdahl K. and Persson-Nilsson K. (2016) Fluorapatite-monazite-allanite relations in the Grängesberg apatite-iron oxide ore district, Bergslagen, Sweden. Am. Mineral. 101, 1769–1782.
- Kestin J., Sengers J. V., Kamgar-Parsi B. and Levelt Sengers J. M. H. (1984) Thermophysical properties of fluid H₂O. J. Phys. Chem. Ref. Data 13, 175–183.
- Kielland J. (1937) Individual activity coefficients of ions in aqueous solutions. J. Am. Chem. Soc. 59, 1675–1678.
- Kohn, M. J., Rakovan, J. and Hughes, J. M. (eds.) (2002)Synthesis, Structure, and Properties of Monazite, Pretulite, and Xenotime. Mineralogical Society of America, Washington, DC.
- Kulik D. A., Wagner T., Dmytrieva S. V., Kosakowski G., Hingerl F. F., Chudnenko K. V. and Berner U. R. (2013) GEM-Selektor geochemical modeling package: revised algorithm and GEMS3K numerical kernel for coupled simulation codes. *Comput. Geosci.* 17, 1–24.
- Li Y., Kowalski P. M., Blanca-Romero A., Vinograd V. and Bosbach D. (2014) Ab initio calculation of excess properties of La_{1-x}(LN, An)_xPO₄ solid solutions. *J. Solid State Chem.* **220**, 137–141.
- Liu X. and Byrne R. H. (1997) Rare earth and yttrium phosphate solubilities in aqueous solution. *Geochim. Cosmochim. Acta* 61, 1625–1633.
- Loges A., Migdisov A. A., Wagner T., Williams-Jones A. E. and Markl G. (2013) An experimental study of the aqueous solubility and speciation of Y(III) fluoride at temperatures up to 250°C. Geochim. Cosmochim. Acta 123, 403–415.
- Louvel M., Bordage A., Testemale D., Zhou L. and Mavrogenes J. (2015) Hydrothermal controls on the genesis of REE deposits: insights from an in situ XAS study of Yb solubility and speciation in high temperature fluids. Chem. Geol. 417, 228–237.
- Lucas S., Champion E., Bregiroux D., Bernache-Assollant D. and Audubert F. (2004) Rare earth phosphate powders RePO₄-nH₂O (Re = La, Ce or Y) Part II. Thermal behavior. *J. Solid State Chem.* 177, 1312–1320.
- Mair P., Tropper P., Harlov D. E. and Manning C. E. (2017) The solubility of CePO₄ monazite and YPO₄ xenotime in KCl-H₂O fluids at 800°C and 1.0 GPa: implications for REE transport in high-grade crustal fluids. *Am. Mineral*.
- Mayanovic R. A., Anderson A. J., Bassett W. A. and Chou I. M. (2007) On the formation and structure of rare-earth element complexes in aqueous solutions under hydrothermal conditions with new data on gadolinium aqua and chloro complexes. *Chem. Geol.* **239**, 266–283.
- Mayanovic R. A., Anderson A. J., Bassett W. A. and Chou I. M. (2009) The structure and stability of aqueous rare-earth elements in hydrothermal fluids: New results on neodymium (III) aqua and chloroaqua complexes in aqueous solutions to 500 °C and 520 MPa. *Chem. Geol.* **259**, 30–38.

- McDonough W. F. and Sun S-. (1995) The composition of the earth. *Chem. Geol.* **120**, 223–253.
- Mesbah A., Clavier N., Elkaim E., Gausse C., Kacem I., Ben Szenknect S. and Dacheux N. (2014) Monoclinic form of the rhabdophane compounds: REEPO₄ 0.667H₂O. Cryst. Growth Des. 14, 5090-5098.
- Mesbah A., Clavier N., Elkaim E., Szenknect S. and Dacheux N. (2017) In pursuit of the rhabdophane crystal structure: from the hydrated monoclinic LnPO₄·0.667H₂O to the hexagonal LnPO₄ (Ln = Nd, Sm, Gd, Eu and Dy). *J. Solid State Chem.* **249**, 221–227.
- Migdisov A. A. and Williams-Jones A. E. (2007) An experimental study of the solubility and speciation of neodymium (III) fluoride in F-bearing aqueous solutions. *Geochim. Cosmochim. Acta* 71, 3056–3069.
- Migdisov A. A. A., Williams-Jones A. E. E. and Wagner T. (2009) An experimental study of the solubility and speciation of the Rare Earth Elements (III) in fluoride- and chloride-bearing aqueous solutions at temperatures up to 300°C. Geochim. Cosmochim. Acta 73, 7087–7109.
- Migdisov A. A., Williams-Jones A. E., van Hinsberg V. and Salvi S. (2011) An experimental study of the solubility of baddeleyite (ZrO₂) in fluoride-bearing solutions at elevated temperature. *Geochim. Cosmochim. Acta* 75, 7426–7434.
- Migdisov A. A. and Williams-Jones A. E. (2014) Hydrothermal transport and deposition of the rare earth elements by fluorine-bearing aqueous liquids. *Miner. Depos.* **49**, 987–997.
- Migdisov A., Williams-Jones A. E., Brugger J. and Caporuscio F. A. (2016) Hydrothermal transport, deposition, and fractionation of the REE: Experimental data and thermodynamic calculations. *Chem. Geol.* 439, 13–42.
- Miron G. D., Kulik D. A., Dmytrieva S. V. and Wagner T. (2015) GEMSFITS: Code package for optimization of geochemical model parameters and inverse modeling. *Appl. Geochem.* 55, 28–45.
- Miron G. D., Wagner T., Kulik D. A. and Heinrich C. A. (2016) Internally consistent thermodynamic data for aqueous species in the system Na-K-Al-Si-O-H-Cl. *Geochim. Cosmochim. Acta* 187, 41–78.
- Miron G. D., Wagner T., Kulik D. A. and Lothenbach B. (2017) An internally consistent thermodynamic dataset for aqueous species in the system Ca-Mg-Na-K-Al-Si-O-H-C-Cl to 800 °C and 5 kbar. *Am. J. Sci.* **317**, 755–806.
- Mooney R. C. L. (1950) X-ray diffraction study of cerous phosphate and related crystals. I. Hexagonal modification. *Acta Crystallogr.* **3**, 337–340.
- Moore M., Chakhmouradian A. R., Mariano A. N. and Sidhu R. (2015) Evolution of rare-earth mineralization in the Bear Lodge carbonatite, Wyoming: Mineralogical and isotopic evidence. *Ore Geol. Rev.* 64, 499–521.
- Navrotsky A., Lee W., Mielewczyk-Gryn A., Ushakov S. V., Anderko A., Wu H. and Riman R. C. (2015) Thermodynamics of solid phases containing rare earth oxides. *J. Chem. Thermo*dyn. 88, 126–141.
- Neumeier S., Kegler P., Arinicheva Y., Shelyug A., Kowalski P. M., Schreinemachers C., Navrotsky A. and Bosbach D. (2017) Thermochemistry of La_{1-x}Ln_xPO₄-monazites (Ln = Gd, Eu). *J. Chem. Thermodyn.* **105**, 396–403.
- Ni Y., Hughes J. M. and Mariano A. N. (1995) Crystal chemistry of the monazite and xenotime structures. Am. Mineral. 80, 21– 26.
- Oelkers E. H. and Poitrasson F. (2002) An experimental study of the dissolution stoichiometry and rates of a natural monazite as a function of temperature from 50 to 230 °C and pH from 1.5 to 10. *Chem. Geol.* **191**, 73–87.

- Paquette J. L. and Tiepolo M. (2007) High resolution (5 μm) U-Th-Pb isotope dating of monazite with excimer laser ablation (ELA)-ICPMS. *Chem. Geol.* **240**, 222–237.
- Perry E. P. and Gysi A. P. (2018) Rare earth elements in mineral deposits: speciation in hydrothermal fluids and partitioning in calcite. *Geofluids* 2018, 21–26.
- Poitrasson F., Chenery S. and Bland D. J. (1996) Contrasted monazite hydrothermal alteration mechanisms and their geochemical implications. *Earth Planet. Sci. Lett.* 145, 79–96.
- Poitrasson F., Hanchar J. M. and Schaltegger U. (2002) The current state and future of accessory mineral research. *Chem. Geol.* **191**, 3–24.
- Poitrasson F., Oelkers E., Schott J. and Montel J.-M. (2004) Experimental determination of synthetic NdPO₄ monazite endmember solubility in water from 21 °C to 300 °C: implications for rare earth element mobility in crustal fluids. *Geochim. Cosmochim. Acta* **68**, 2207–2221.
- Popa K. and Konings R. J. M. (2006) High-temperature heat capacities of EuPO₄ and SmPO₄ synthetic monazites. *Ther-mochim. Acta* 445, 49–52.
- Popa K., Konings R. J. M. and Geisler T. (2007) High-temperature calorimetry of (La_{1x}Ln_x)PO₄ solid solutions. *J. Chem. Thermo-dyn.* 39, 236–239.
- Popa K., Sedmidubský D., Beneš O., Thiriet C. and Konings R. J. M. (2006) The high-temperature heat capacity of LnPO₄ (Ln = La, Ce, Gd) by drop calorimetry. *J. Chem. Thermodyn.* 38, 825–829.
- Pourtier E. and Devidal J. (2010) Solubility measurements of synthetic neodymium monazite as a function of temperature at 2 kbars, and aqueous neodymium speciation in equilibrium with monazite. *Geochim. Cosmochim. Acta* 74, 1872–1891.
- Pyle J. M., Spear F. S., Rudnick R. L. and Mcdonough W. F. (2001) Monazite xenotime garnet equilibrium in metapelites and a new monazite garnet thermometer. *J. Petrol.* **42**, 2083–2107.
- Richter L., Diamond L. W., Atanasova P., Banks D. A. and Gutzmer J. (2018) Hydrothermal formation of heavy rare earth element (HREE)–xenotime deposits at 100 °C in a sedimentary basin. *Geology*, 263–266.
- Robinson R. A. and Stokes R. H. (1968) *Electrolyte Solutions*. Butterworths, London.
- Roncal-Herrero T., Rodríguez-Blanco J. D., Oelkers E. H. and Benning L. G. (2011) The direct precipitation of rhabdophane (REEPO4·H2O) nanorods from acidic aqueous solutions at 5–100 °C. J. Nanoparticle Res. 13, 4049–4062. https://doi.org/ 10.1007/s11051-011-0347-6.
- Salvi S. and Williams-Jones A. E. (1990) The role of hydrothermal processes in the granite-hosted Zr, Y, REE deposit at Strange Lake, Quebec/Labrador: evidence from fluid inclusions. *Geochim. Cosmochim. Acta* 54, 2403–2418.
- Samson I., Wood S. and Finucane K. (2004) Fluid inclusion characteristics and genesis of the fluorite-parisite mineralization in the Snowbird deposit, Montana. *Econ. Geol.* 99, 1727–1744.
- Shock E. L. and Helgeson H. C. (1988) Calculation of the thermodynamic and transport properties of aqueous species at high pressures and temperatures: Correlation algorithms for ionic species and equation of state predictions to 5 kb and 1000° C. Geochim. Cosmochim. Acta 52, 2009–2036.
- Shock E. L., Helgeson H. C. and Sverjensky D. A. (1989) Calculation of the thermodynamic and transport properties of aqueous species at high pressures and temperatures: standard partial molal properties of inorganic neutral species. *Geochim. Cosmochim. Acta* 53, 2157–2183.
- Shock E. L., Oelkers E. H., Johnson S. J. W., Sverjensky D. A. and Helgeson H. C. (1992) Calculation of the thermodynamic

- properties of aqueous species at high pressures and temperatures. J. Chem. Soc. Faraday Trans. 88, 803–826.
- Shock E. L., Sassani D. C., Willis M. and Sverjensky D. A. (1997) Inorganic species in geologic fluids: correlations among standard molal thermodynamic properties of aqueous ions and hydroxide complexes. *Geochim. Cosmochim.* 61, 907–950.
- Smith M. P., Henderson P. and Campbell L. S. (2000) Fractionation of the REE during hydrothermal processes: constraints from the Bayan Obo Fe-REE-Nb deposit, Inner Mongolia, China. *Geochim. Cosmochim. Acta* 64, 3141–3160.
- Spear F. S. and Pyle J. M. (2002) Apatite, monazite, and xenotime in metamorphic rocks. Rev. Mineral. Geochem. 48, 293–335.
- Tananaev I. V. and Vasil'eva V. P. (1963) Lanthanum phosphates. Russ. J. Inorg. Chem. 8, 555–558.
- Tanger J. C. and Helgeson H. C. (1988) Calculation of the thermodynamic and transport properties of aqueous species at high pressures and temperatures; revised equations of state for the standard partial molal properties of ions and electrolytes. *Am. J. Sci.* 288, 19–98.
- Teufel S. and Heinrich W. (1997) Partial resetting of the U-Pb isotope system in monazite through hydrothermal experiments: an SEM and U-Pb isotope study. *Chem. Geol.* **137**, 273–281.
- Thiriet C., Konings R. J. M., Javorský P. and Magnani N. (2005) The low temperature heat capacity of LaPO₄ and GdPO₄, the thermodynamic functions of the monazite-type LnPO₄ series. *J. Chem. Thermodyn.* **37**, 131–139.
- Thiriet C., Konings R. J. M., Javorský P. and Wastin F. (2004) The heat capacity of cerium orthophosphate CePO₄, the synthetic analogue of monazite. *Phys. Chem. Miner.* **31**, 347–352.
- Trofanenko J., Williams-Jones A. E., Simandl G. J. and Migdisov A. A. (2016) The nature and origin of the REE mineralization in the Wicheeda Carbonatite, British Columbia, Canada. *Econ. Geol.* 111, 199–223.
- Tropper P., Manning C. E. and Harlov D. E. (2013) Experimental determination of CePO₄ and YPO₄ solubilities in H₂O-NaF at 800°C and 1 GPa: implications for rare earth element transport in high-grade metamorphic fluids. *Geofluids* 13, 372–380.
- Tropper P., Manning C. E. and Harlov D. E. (2011) Solubility of CePO₄ monazite and YPO₄ xenotime in H₂O and H₂O–NaCl at 800°C and 1GPa: implications for REE and Y transport during high-grade metamorphism. *Chem. Geol.* **282**, 58–66.
- Tsay A., Zajacz Z. and Sanchez-Valle C. (2014) Efficient mobilization and fractionation of rare-earth elements by aqueous fluids upon slab dehydration. *Earth Planet. Sci. Lett.* 398, 101–112.
- Ushakov S. V., Helean K. B., Navrotsky A. and Boatner L. A. (2001) Thermochemistry of rare-earth orthophosphates. *J. Mater. Res.* **16**, 2623–2633.
- Vasyukova O. V. and Williams-Jones A. E. (2018) Direct measurement of metal concentrations in fluid inclusions, a tale of hydrothermal alteration and REE ore formation from Strange Lake, Canada. *Chem. Geol.* 483, 385–396.
- Vasyukova O. V., Williams-Jones A. E. and Blamey N. J. F. (2016) Fluid evolution in the Strange Lake granitic pluton, Canada: implications for HFSE mobilisation. *Chem. Geol.* 444, 83–100.
- Wagner T., Kulik D. A., Hingerl F. F. and Dmytrieva S. V. (2012) GEM-Selektor geochemical modeling package: TSolMod library and data interface for multicomponent phase models. Can. Mineral. 50, 1173–1195.
- Wall F., Niku-Paavola V. N., Storey C., Müller A. and Jeffries T. (2008) Xenotime-(Y) from carbonatite dykes at Lofdal, Namibia: unusually low LREE: HREE ratio in carbonatite, and the first dating of xenotime overgrowths on zircon. *Can. Mineral.* 46, 861–877.
- Wilkinson T. M., Wu D., Musselman M. A., Li N., Mara N. and Packard C. E. (2017) Mechanical behavior of rare-earth

- orthophosphates near the monazite/xenotime boundary characterized by nanoindentation. *Mater. Sci. Eng. A* **691**, 203–210.
- Williams-Jones A. E., Samson I. M. and Olivo G. R. (2000) The genesis of hydrothermal fluorite-REE deposits in the Gallinas Mountains, New Mexico. *Econ. Geol.* **95**, 327–341.
- Williams-Jones A. E., Migdisov A. A. and Samson I. M. (2012) Hydrothermal mobilisation of the rare earth elements a tale of "Ceria" and "Yttria". *Elements* 8, 355–360.
- Williams M. L., Jercinovic M. J., Harlov D. E., Budzyń B. and Hetherington C. J. (2011) Resetting monazite ages during fluidrelated alteration. *Chem. Geol.* 283, 218–225.
- Wood S. (1990) The aqueous geochemistry of the rare-earth elements and yttrium: 2. Theoretical predictions of speciation in hydrothermal solutions to 350 °C at saturation water vapor pressure. *Chem. Geol.* **88**, 99–125.
- Wood S. A., Palmer D. A., Wesolowski D. J. and Bénézeth P. (2002) The aqueous geochemistry of the rare earth elements and yttrium. Part XI. The solubility of Nd(OH)₃ and hydrolysis of Nd³⁺ from 30 to 290 °C at saturated water vapor pressure with in-situ pHm measurement. Water-rock Interact. Ore Depos. Environ. Geochem. Tribut. David Crerar Spec. Publ. 7, 229–256.
- Zhou L., Mavrogenes J., Spandler C. and Li H. (2016) A synthetic fluid inclusion study of the solubility of monazite-(La) and xenotime-(Y) in H₂O-Na-K-Cl-F-CO₂ fluids at 800 °C and 0.5 GPa. *Chem. Geol.* **442**, 121–129.

Associate editor: Rosemary Hickey-Vargas